Mon. Not. R. Astron. Soc. **294,** 642–656 (1998)

A comprehensive variability study of the enigmatic WN8 stars: final results

S. V. Marchenko,[1★] A. F. J. Moffat,[1★] T. Eversberg,[1★] G. M. Hill,[1,2★] G. H. Tovmassian,[3★] T. Morel[1★] and W. Seggewiss[4★]

[1]*Département de Physique, Université de Montreal, C.P. 6128, Succursale Centre-Ville, Montreal, Quebec, H3C 3J7, Canada, and Observatoire du Mont Mégantic*
[2]*Dominion Astrophysical Observatory, 5071 W. Saanich Road, Victoria, BC, V8X4M6, Canada*
[3]*Instituto de Astronomía, Apartado Postal 877, C.P. 22860, Ensenada, Mexico*
[4]*Universitäts-Sternwarte Bonn, Auf dem Hügel 71, D-53121, Bonn, Germany*

Accepted 1997 September 26. Received 1997 September 10; in original form 1997 May 30

ABSTRACT

As a conclusion of our all-sky variability survey of the 'enigmatic' variable WN8 stars, we have carried out coordinated multisite photometric and spectroscopic observations of WN8 stars in 1989 and 1994–1995. We confirm the leading role of the stellar core in restructuring the whole wind. This emerges as a *statistical* trend: the higher the level of the ∼continuum (i.e. ∼core) light variations, the higher the variability of the P Cygni edges of the optical emission lines. However, the form of the correlation between the light and profile variations is generally different for each individual star. The high level of activity of WN8 stars may be supported/induced by pulsational instability.

Key words: stars: variables: other – stars: Wolf–Rayet.

1 INTRODUCTION

WN8 stars are the direct evolutionary descendants of massive and luminous Of stars (Maeder 1996; Crowther & Smith 1997). They possess some properties that distinguish them from the general Wolf–Rayet (WR) population. (a) They consistently demonstrate the highest level of omnipresent intrinsic variability (Lamontagne & Moffat 1987; Robert et al. 1989; Antokhin et al. 1995). (b) Their binary frequency is very low (Moffat 1989). Apart from the extremely wide wind-interacting visual binary WR 147 (WN8 + B0.5 V; Williams et al. 1997; Niemela et al. 1997), claims of suspected short-period binarity among WN8 stars have been mainly based on light-curve variations. The best examples are HD 96548 = WR 40, with two prevailing periodicities in light variations, $P = 12.3$ and 17.5 d, interpreted as binary orbital revolution and axial rotation of the WR component (Matthews & Moffat 1994), and HD 134819 = WR 66, with a clear periodicity of 3.51 h (Antokhin et al. 1995), independently confirmed by Rauw et al. (1996). In general, the search for coherency in radial velocity and light variations has led to controversial results (Massey & Conti 1980; Lamontagne, Moffat & Seggewiss 1983). (c) Some WN8 stars have large distances from the Galactic plane, far exceeding the scale height $|z| \sim 60$ pc for Galactic WR Population I stars (Moffat & Isserstedt 1980; van der Hucht et al. 1988). (d) WN8 stars avoid stellar clusters and associations. (e) Some WN8 stars have high runaway speeds (Moffat et al. 1997).

Taken together, these five facts have led many authors to a logical conclusion: some (if not all) WN8 stars may be runaway objects after a supernova recoil

We started our systematic survey of WN8 stars in 1989, with more intense follow-up in 1993 (Marchenko et al. 1994; Antokhin et al. 1995), in an attempt to sample adequately the light variations on time-scales of hours–weeks and search for any periodic phenomena which may be attributed to binarity. Here we report our 1994–1995 observations, thus completing our all-sky variability survey of bright, $m(V) \leq 13$ mag, WN8 stars. In 1995 we decided to include in

★E-mail: sergey@astro.umontreal.ca (SVM);
moffat@astro.umontreal.ca (AFJM);
eversber@astro.umontreal.ca (TE);
morel@astro.umontreal.ca (TM);
ghill@dao.nrc.ca (GHM);
gag@bufadora.astrosen.unam.mx (GHT);
seggewis@astro.uni-bonn.de (WS)

our sample one more star, WR 98, as an example of a possible binary (Niemela 1991) with hybrid WN7/WC7 spectrum and suspected high level of variability. For a first compilation of a list of objects, we started with the spectral subtypes from van der Hucht et al. (1988), being aware that further attempts at reclassification may change the assigned spectral subclass by as much as a subclass (e.g. Smith, Shara & Moffat 1996). This led us to include WR 120 and 148 in our sample, with the latter as a good example of an SB1 system (Marchenko et al. 1996).

2 OBSERVATIONS AND DATA REDUCTION

2.1 Photometry

We obtained 10 nights of photometry for WR 40 in 1989 using the 0.5-m telescope of ESO (Chile). The remaining programme stars were observed photometrically for 1 month in 1994 and 2 months in 1995 via two-site broad-band V photometry: at the 0.84-m telescope of the San Pedro Martir (SPM) Observatory, Mexico, and the 0.6-m telescope of the Crimean (Ukraine) Observational Station of GAISH. The extinction coefficients were derived using numerous observations at each site of comparison stars for WR 123, 124, 130 and 148. For the SPM data, we found and applied $k_V = 0.277$ for 1994 June–July, $k_V = 0.258 \pm 0.018$ for 1995 June 21–30, $k_V = 0.141 \pm 0.004$ for 1995 July 1 to August 3 and $k_V = 0.226 \pm 0.017$ for 1995 August 4–18. All the observations from Crimea were reduced into the SPM system by adjusting zero-points calculated from the overlapping data subsets. General information about the observed stars is provided in Table 1, where $\sigma(V)$ refers to $[a_1\sigma(wr-c1) + a_2\sigma(wr-c2)]/(a_1 + a_2)$ for the WR star relative to the non-variable comparison stars ($a_i = 1$ if constant, $a_i = 0$ if variable), or $\sigma(c2 - c1)$ for the comparison stars, after allowing for variability of the comparison (if any). The equinox 2000.0 coordinates were measured using the STScI Digitized Sky Survey and its software. The spectral types and narrow-band ($\sim$continuum) visual v magnitudes for WR stars are taken from van der Hucht et al. (1988) and from Smith et al. (1996; values in brackets in our Table 1). The individual observations are given in Tables 2–11. Note that we have not corrected the original data in Tables 2–11 for variability of the comparison stars (see Table 1 for details).

2.2 Spectroscopy

We supplemented our photometry by quasi-simultaneous spectroscopy. We obtained three nights of CASPEC echelle spectroscopy [$\lambda\lambda$5000–6000 Å; resolution $\Delta\lambda = 0.2$ Å (2 pixels); signal-to-noise ratio S/N $\geqq 200$] for WR 40 in 1989 using the 3.6-m telescope of ESO (Chile). Additionally, three stars (WR 123, 124 and 156) were observed spectroscopically from two sites: the 1.6-m telescope of the Observatoire du Mont Mégantic, Canada with attached Cassegrain spectrograph and Thompson 1024 × 1024 pixel CCD [$\lambda\lambda = 4350$–6000 Å; $\Delta\lambda = 4.9$ Å (3 pixels); S/N $\geqq 150$ in the stellar continuum for a 1.0–1.5 h exposure], and the 1.8-m telescope of the Dominion Astrophysical Observatory, Canada, equipped with a Cassegrain spectrograph and SITe 1024 × 1024 pixel CCD [$\lambda\lambda = 3650$–5250 Å; $\Delta\lambda = 4.6$ Å (3 pixels); typical S/N $\geqq$ 150–250 in the stellar continuum was reached in 1–2 h. The observations of WR 123, 124 and 156 extend through 1995 May to October – cf. the journals of observation in Tables 12–14. The data reduction was performed using standard IRAF facilities. Comprehensive co-alignment of the spectra using all available prominent interstellar lines, as well as relatively strong night-sky emissions, enables us to reach relatively high (even for the given low spectral resolution) precision in radial velocity: $\sigma(RV) = 3$–12 km s^{-1}, depending on the star. All listed heliocentric radial velocities (Tables 12–14) were measured by cross-correlating individual spectra with the mean spec-

Table 1. Summary of the photometric observations.

Star	Spectral type	v mags	α(2000) h m s	δ(2000) ° ′ ″	σ(V) mags	Variability Period (days)	Variability Ampl.(mags)
WR 40	WN8(WN8h)	7.85	11 06 17.2	-65 30 35	0.019	var.	Irreg.?
c6=HD96568	A3V	6.4	11 06 24.6	-64 50 22	0.003	const	–
c7=HD96287	B9.5V	7.2	11 04 50.2	-64 36 56	0.003	const	–
WR 98	WN7/C7(WN 8o/C7)	12.51	17 37 13.7	-33 27 56	0.032	var.	Irreg.
c1=HDE318021	F0		17 38 7.0	-33 29 40	0.004	const	–
c2			17 37 25.8	-33 29 43	0.004	const	–
WR 105	WN8 (WN9h)	12.92	18 02 23.4	-23 34 38	0.018	4.13:	0.019:
c2=LS4564	B		18 01 57.7	-23 33 26	0.006	const	–
c3			18 02 23.3	-23 33 29	0.006	const	–
WR 116	WN8 (WN8h)	13.38	18 27 04.2	-12 22 51	0.034	5.78	0.043
c2			18 27 11.4	-12 28 24	–	2.70	0.018
c3			18 27 15.7	-12 29 55	0.006	∼const	–
WR 120	WN7 (WN7o)	12.30	18 41 00.8	-4 26 14	0.036	6.90:	0.042:
c1			18 40 43.4	-4 23 24	0.004	const	–
c2			18 40 38.9	-4 22 20	0.004	const	–
WR 123	WN8 (WN8o)	11.26	19 03 58.9	-4 19 02	0.029	multiple	–
c1=BD-04 4680	K0		19 04 27.4	-4 25 53	0.007	const	–
c2			19 04 15.2	-4 16 27	0.007	const	–
WR 124	WN8 (WN8h)	11.58	19 11 30.9	16 51 38	0.018	4.45, 1.70	0.019, 0.017
c3			19 10 58.5	16 50 05	–	14.6	0.016
c5			19 12 04.9	16 46 50	0.006	const	–
WR 130	WN8 (WN8h)	12.60	19 59 12.8	31 27 10	0.017	4.16:	0.017:
c2=BD+31 3872B	G5		19 59 04.7	31 28 00	0.010	0.88?	0.004
c3=HDE331627	G5		19 59 05.3	31 27 38	0.010	const?	–
WR 148	WN7 (WN8h)	10.46	20 41 21.6	52 35 16	0.016	4.32	0.030
c1			20 40 49.5	52 33 14	0.004	const	–
c2			20 41 05.0	52 28 28	0.004	const	–
WR 156	WN8 (WN8h)	11.09	23 00 10.2	60 55 39	0.017	15.6(14.4)	0.023(0.019)
c2			23 00 23.6	60 53 22	0.005	const	–
c3			23 00 20.4	60 58 12	0.005	const	–

Table 2. Photometric observations of WR 40.

HJD-2447000	wr-c6 Δy	wr-c6 Δb	c7-c6 Δy	c7-c6 Δb	wr-c6 $\Delta(b-y)$
672.623	1.309	1.080	0.844	0.795	-0.229
673.492	1.337	1.096	0.835	0.785	-0.241
673.542	1.336	1.099	0.840	0.793	-0.237
673.588	1.326	1.090	0.832	0.785	-0.236
673.642	1.334	1.096	0.840	0.786	-0.238
673.682	1.321	1.093	0.837	0.791	-0.228
673.714	1.323	1.091	0.840	0.785	-0.232
674.493	1.351	1.103	0.842	0.793	-0.248
674.526	1.337	1.091	0.836	0.779	-0.246
675.623	1.300	1.077	0.838	0.786	-0.223
675.677	1.299	1.073	0.842	0.793	-0.226
676.488	1.332	1.085	0.839	0.787	-0.247
676.521	1.327	1.088	0.838	0.784	-0.239
676.554	1.329	1.089	0.835	0.786	-0.240
676.604	1.327	1.087	0.833	0.787	-0.240
676.653	1.325	1.089	0.839	0.791	-0.236
676.679	1.324	1.087	0.840	0.793	-0.237
677.479	1.335	1.120	0.839	0.790	-0.215
677.505	1.343	1.123	0.840	0.788	-0.220
677.528	1.345	1.128	0.834	0.786	-0.217
677.573	1.352	1.130	0.836	0.787	-0.222
677.623	1.351	1.132	0.839	0.789	-0.219
677.673	1.348	1.126	0.842	0.793	-0.222
677.711	1.344	1.122	0.841	0.790	-0.222
678.489	1.320	1.081	0.841	0.790	-0.239
678.515	1.318	1.080	0.839	0.786	-0.238
678.537	1.315	1.081	0.834	0.788	-0.234
678.589	1.327	1.080	0.845	0.788	-0.247
678.636	1.331	1.079	0.841	0.792	-0.252
678.698	1.327	1.075	0.838	0.787	-0.252
679.713	1.295	1.066	0.837	0.794	-0.229
679.725	1.290	1.063	0.839	0.790	-0.227
679.736	1.292	1.057	0.846	0.787	-0.235
680.488	1.296	1.051	0.841	0.782	-0.245
680.540	1.294	1.060	0.842	0.791	-0.234
680.591	1.303	1.058	0.838	0.787	-0.245
680.683	1.287	1.062	0.834	0.788	-0.225
681.615	1.297	1.059	0.830	0.786	-0.238
681.657	1.295	1.066	0.838	0.795	-0.229

Note: all data were obtained at the European Southern Observatory.

Table 3. Photometric observations of WR 98.

HJD-2449000	wr-c1 ΔV	wr-c2 ΔV	c2-c1 ΔV	HJD-2449000	wr-c1 ΔV	wr-c2 ΔV	c2-c1 ΔV
894.7673	2.446	1.948	0.498	924.8054	2.422	1.929	0.493
895.7438	2.468	1.970	0.498	925.7050	2.426	1.936	0.490
897.8215	2.430	1.940	0.490	925.8221	2.430	1.930	0.500
898.8052	2.426	1.932	0.494	926.7055	2.462	1.961	0.501
899.7956	2.492	2.000	0.492	926.8190	2.447	1.954	0.493
900.7920	2.459	1.970	0.489	927.6958	2.463	1.971	0.492
902.8140	2.440	1.949	0.491	928.7036	2.474	1.979	0.495
903.8038	2.475	1.980	0.495	929.7018	2.468	1.972	0.496
904.7964	2.450	1.962	0.488	929.8064	2.452	1.958	0.494
905.7847	2.461	1.964	0.497	930.6981	2.453	1.960	0.493
907.8266	2.393	1.895	0.498	930.8037	2.452	1.964	0.488
911.7564	2.458	1.966	0.492	931.6981	–	1.930	–
912.7542	2.416	1.929	0.487	934.7201	2.468	1.977	0.491
913.7432	2.477	1.987	0.490	935.6805	2.396	1.905	0.491
915.7505	2.455	1.960	0.495	938.6851	2.349	1.851	0.498
920.7308	2.464	1.972	0.492	944.6751	2.406	1.904	0.502
921.7970	2.460	1.968	0.492	945.6777	2.478	1.986	0.492
922.6968	2.506	2.011	0.495	946.6718	2.462	1.969	0.493
923.6948	2.466	1.974	0.492	947.6659	2.516	2.021	0.495
924.7031	2.432	1.934	0.498				
924.8054	2.422	1.929	0.493				

Note: all data were obtained at the San Pedro Martir Observatory.

trum of the given star (Fig. 1) via the task 'fxcor' in IRAF. The precision of the radial velocities was calculated by cross-correlating the mean spectrum with 3–4 segments, 300–400 Å each, of the individual spectrum and estimating the resulting scatter in RV.

Table 4. Photometric observations of WR 105.

HJD-2449000	wr-c3 ΔV	wr-c2 ΔV	c2-c3 ΔV	HJD-2449000	wr-c3 ΔV	wr-c2 ΔV	c2-c3 ΔV
520.8232	–	1.102	–	915.7869	1.318	1.024	0.294
521.8050	–	1.057	–	918.7842	1.366	1.074	0.292
522.8100	–	1.054	–	920.8551	1.345	1.038	0.307
533.8017	–	1.058	–	921.8101	1.339	1.044	0.295
537.7074	–	1.052	–	922.7102	1.331	1.035	0.296
538.7846	–	1.026	–	922.8329	1.330	1.032	0.298
540.8083	–	1.054	–	923.7078	1.335	1.043	0.292
541.7735	–	1.051	–	923.8059	1.340	1.029	0.311
543.7647	–	1.070	–	924.7151	1.326	1.034	0.292
890.8644	1.326	1.023	0.303	924.8294	1.368	1.076	0.292
891.8197	1.364	1.068	0.296	925.7155	1.344	1.047	0.297
894.7385	1.344	1.054	0.290	925.8330	1.350	1.060	0.290
895.7259	1.333	1.034	0.299	926.7161	1.344	1.049	0.295
897.8427	1.330	1.034	0.296	926.8310	1.324	1.039	0.285
898.7876	1.344	1.050	0.294	927.7056	1.337	1.032	0.305
899.7774	1.350	1.056	0.294	927.7738	1.316	1.006	0.310
899.8864	1.348	1.050	0.298	928.7140	1.356	1.058	0.298
900.7765	1.345	1.049	0.296	928.8499	1.347	1.057	0.290
901.7927	1.343	1.051	0.292	929.7121	1.317	1.026	0.291
902.7761	1.338	1.044	0.294	929.8186	1.347	1.057	0.290
902.8946	1.339	1.039	0.300	930.7080	1.331	1.026	0.305
903.7788	1.368	1.066	0.302	930.8143	1.325	1.035	0.290
903.8954	–	1.073	–	931.7078	1.342	1.040	0.302
904.7330	1.359	1.055	0.304	931.8242	1.339	1.044	0.295
904.8521	1.343	1.043	0.300	932.7832	1.343	1.043	0.300
905.7573	1.329	1.036	0.293	934.7331	1.309	1.007	0.302
905.8731	1.322	1.027	0.295	943.7036	1.291	0.999	0.292
907.8081	1.352	1.057	0.295	944.6906	1.336	1.049	0.287
911.7428	1.340	1.034	0.306	945.6912	1.352	1.054	0.298
912.7223	1.339	1.042	0.297	946.6867	1.331	1.034	0.297
913.7097	1.320	1.019	0.301	947.6800	1.335	1.046	0.289

Note: all data were obtained at the San Pedro Martir Observatory.

Table 5. Photometric observations of WR 116.

HJD-2449000	Obs.	wr-c3 ΔV	wr-c2 ΔV	c2-c3 ΔV	HJD-2449000	Obs.	wr-c3 ΔV	wr-c2 ΔV	c2-c3 ΔV
519.8440	S	1.877	1.141	0.736	906.9017	S	1.794	1.073	0.721
521.9677	S	1.803	1.079	0.734	907.7898	S	1.789	1.047	0.742
522.9283	S	1.744	1.010	0.734	907.9265	S	1.849	1.110	0.739
533.8152	S	1.756	1.020	0.703	908.7477	S	1.770	1.036	0.734
536.7757	S	1.818	–	–	918.7410	S	1.787	1.041	0.746
537.8120	S	1.806	–	–	920.7126	S	1.797	1.084	0.713
538.8070	S	1.767	–	–	920.8929	S	1.775	1.033	0.742
540.8581	S	1.764	–	–	921.6885	S	1.800	1.081	0.719
541.7937	S	1.778	–	–	921.8263	S	1.789	1.045	0.744
542.8658	S	1.807	–	–	922.7262	S	1.693	0.987	0.706
543.7858	S	1.780	–	–	922.8495	S	1.791	1.088	0.703
544.7550	S	1.782	–	–	923.7232	S	1.815	1.088	0.727
885.4388	G	1.790	1.051	0.738	923.8218	S	1.799	1.086	0.713
886.4806	G	1.843	1.079	0.760	924.7282	S	1.794	1.060	0.734
890.8316	S	1.781	1.035	0.746	924.8448	S	1.818	1.080	0.738
892.3826	G	1.735	1.032	0.702	925.7290	S	1.774	1.056	0.718
892.8246	S	1.796	1.068	0.727	925.8465	S	1.771	1.054	0.717
893.3948	G	1.738	1.000	0.738	926.7302	S	1.766	1.030	0.736
893.8180	S	1.770	1.022	0.748	926.8447	S	1.775	1.033	0.742
894.8177	S	1.804	1.087	0.717	927.7185	S	1.785	1.055	0.730
895.3875	G	1.826	1.095	0.731	928.7270	S	1.802	1.072	0.730
895.7947	S	1.833	1.110	0.723	928.8661	S	1.778	1.028	0.750
897.3992	G	1.782	1.053	0.728	929.7235	S	1.800	1.063	0.737
897.8014	S	1.770	1.038	0.732	929.8327	S	1.848	1.114	0.734
898.7860	S	1.723	1.003	0.720	930.7204	S	1.917	1.201	0.716
899.7572	S	1.776	1.034	0.742	930.8146	S	1.800	1.080	0.720
900.7570	S	1.770	1.035	0.735	931.7202	S	1.793	1.065	0.728
900.9066	S	1.764	1.047	0.717	931.8372	S	1.798	1.061	0.737
901.3918	G	1.796	1.046	0.732	932.7970	S	1.826	1.091	0.735
901.7751	S	1.764	1.042	0.722	934.7483	S	1.782	1.045	0.737
902.4017	G	1.755	1.028	0.728	934.8403	S	1.770	1.027	0.743
902.7590	S	1.766	1.026	0.740	935.7408	S	1.798	1.076	0.722
902.9114	S	1.769	1.039	0.730	935.8243	S	1.867	1.128	0.739
903.3734	G	1.795	1.056	0.740	943.7193	S	1.786	1.076	0.710
903.8776	S	1.770	1.048	0.722	944.7063	S	1.800	1.073	0.727
904.7647	S	1.751	1.023	0.728	945.7070	S	1.809	1.057	0.752
904.8695	S	1.779	1.053	0.726	946.7043	S	1.820	1.100	0.720
905.7418	S	1.763	1.015	0.748	947.6953	S	1.810	1.070	0.740
905.8544	S	1.759	1.002	0.757					

Letter S marks the data from the San Pedro Martir Observatory and letter G denotes the data from the Crimean station of the GAISH.

Table 6. Photometric observations of WR 120.

HJD-2449000	wr-c1 ΔV	wr-c2 ΔV	c2-c1 ΔV	HJD-2449000	wr-c1 ΔV	wr-c2 ΔV	c2-c1 ΔV
894.7208	1.439	0.897	0.542	923.8345	1.447	0.905	0.542
895.6959	1.449	0.907	0.545	924.7408	1.460	0.915	0.545
897.7819	1.465	0.924	0.541	924.8600	1.453	0.909	0.544
898.7118	1.503	0.967	0.536	925.7432	1.478	0.934	0.544
898.8764	1.528	0.986	0.542	925.8592	1.422	0.881	0.541
899.7176	1.488	0.946	0.542	926.7428	1.466	0.926	0.540
900.7329	1.502	0.958	0.544	926.8596	1.445	0.897	0.548
900.9245	1.508	0.967	0.541	927.7306	1.408	0.867	0.541
901.7287	1.480	0.930	0.550	928.7430	1.461	0.915	0.546
902.7387	1.477	0.937	0.540	928.8779	1.436	0.896	0.540
902.8787	1.511	0.966	0.545	929.7353	1.481	0.936	0.545
903.7445	1.434	0.892	0.542	929.8550	1.426	0.890	0.536
903.8628	1.430	0.887	0.543	930.7325	1.402	0.858	0.544
904.7806	1.478	0.934	0.544	930.8494	1.410	0.865	0.545
904.8906	1.524	0.975	0.549	930.9194	1.421	0.871	0.551
905.7246	1.492	0.948	0.544	931.7321	1.434	0.898	0.536
905.8366	1.502	0.966	0.536	931.8498	1.378	0.838	0.540
906.9284	1.496	0.952	0.544	931.9204	1.394	0.858	0.536
907.7743	1.518	0.975	0.543	932.8112	1.493	0.949	0.544
907.9470	1.510	0.969	0.541	933.9001	1.517	0.978	0.539
908.7255	1.497	0.949	0.548	934.7606	1.478	0.937	0.541
911.8171	1.470	0.928	0.542	934.8528	1.478	0.931	0.547
912.7386	1.527	0.985	0.542	934.9217	1.463	0.917	0.546
913.7259	1.471	0.926	0.545	935.7534	1.440	0.898	0.542
915.8054	1.444	0.902	0.543	935.8499	1.464	0.918	0.546
918.8145	1.496	0.952	0.544	936.7953	1.434	0.897	0.537
920.8379	1.508	0.960	0.548	938.7206	1.411	–	–
920.9155	1.474	0.940	0.534	943.7451	1.438	0.895	0.543
921.7034	1.464	0.920	0.544	944.7311	1.474	0.930	0.544
921.8424	1.454	0.912	0.542	945.7215	1.430	0.890	0.540
922.7402	1.414	0.872	0.542	946.7229	1.452	0.911	0.541
922.8724	1.450	0.908	0.542	947.7108	1.407	0.866	0.541
923.7375	1.486	0.946	0.540	948.7102	1.432	0.895	0.537

Note: all data were obtained at the San Pedro Martir Observatory.

Table 7. Photometric observations of WR 123.

HJD-2449000	Obs.	wr-c1 ΔV	wr-c2 ΔV	c2-c1 ΔV	HJD-2449000	Obs.	wr-c1 ΔV	wr-c2 ΔV	c2-c1 ΔV
521.8724	S	1.293	-0.323	1.616	912.7803	S	1.321	-0.292	1.613
522.8407	S	1.317	-0.303	1.620	912.8658	S	1.291	-0.313	1.605
525.8314	S	1.331	-0.280	1.610	913.7690	S	1.281	-0.339	1.620
526.8066	S	1.295	-0.331	1.628	913.8744	S	1.273	-0.346	1.619
531.4320	G	1.322	-0.297	1.619	915.8233	S	1.307	-0.302	1.610
533.4401	G	1.346	-0.275	1.621	918.7987	S	1.310	-0.308	1.618
533.8615	S	1.314	-0.306	1.620	920.7526	S	1.231	-0.373	1.604
534.4499	G	1.272	-0.342	1.614	920.9325	S	1.297	-0.308	1.605
536.7992	S	1.355	-0.262	1.617	921.7152	S	1.339	-0.283	1.622
537.7854	S	1.256	-0.354	1.610	921.8550	S	1.280	-0.340	1.620
538.8610	S	1.329	-0.286	1.615	921.9478	S	1.279	-0.345	1.622
540.9186	S	1.318	-0.303	1.620	922.7524	S	1.284	-0.338	1.622
541.8146	S	1.285	-0.334	1.619	922.8862	S	1.258	-0.356	1.614
542.8914	S	1.300	-0.317	1.617	923.6807	S	1.248	-0.366	1.614
543.8029	S	1.342	-0.271	1.613	923.8450	S	1.237	-0.390	1.627
544.7704	S	1.251	-0.368	1.619	923.9336	S	1.289	-0.310	1.599
885.4650	G	1.362	-0.262	1.624	924.6821	S	1.306	-0.312	1.617
886.4905	G	1.333	-0.294	1.627	924.7497	S	1.291	-0.326	1.617
891.7593	S	1.340	-0.272	1.612	924.8706	S	1.297	-0.316	1.613
891.9690	S	1.350	-0.266	1.616	925.6807	S	1.258	-0.355	1.612
892.3570	G	1.350	-0.273	1.623	925.7523	S	1.251	-0.353	1.604
892.7784	S	1.252	-0.356	1.608	925.8686	S	1.251	-0.365	1.616
893.3837	G	1.299	-0.315	1.614	926.6808	S	1.305	-0.316	1.621
893.8330	S	1.314	-0.304	1.620	926.7622	S	1.285	-0.318	1.603
894.7810	S	1.313	-0.297	1.610	926.8927	S	1.258	-0.350	1.608
894.9088	S	1.315	-0.301	1.616	927.7393	S	1.312	-0.306	1.618
895.3668	G	1.342	-0.272	1.614	928.6788	S	1.293	-0.314	1.607
895.7574	S	1.333	-0.284	1.617	928.8087	S	1.297	-0.315	1.612
897.3893	G	1.269	-0.330	1.599	929.6781	S	1.348	-0.274	1.622
897.7624	S	1.272	-0.344	1.616	929.7602	S	1.347	-0.271	1.618
897.9446	S	1.314	-0.298	1.612	929.8639	S	1.342	-0.288	1.630
898.7261	S	1.358	-0.260	1.618	930.6747	S	1.283	-0.322	1.605
898.8566	S	1.334	-0.278	1.612	930.7589	S	1.295	-0.317	1.612
899.7407	S	1.315	-0.304	1.619	930.8580	S	1.300	-0.312	1.612
899.8687	S	1.256	-0.357	1.613	931.6747	S	1.289	-0.325	1.614
900.7176	S	1.272	-0.336	1.608	931.7574	S	1.291	-0.328	1.619
900.8636	S	1.338	-0.269	1.607	931.8689	S	1.290	-0.322	1.612
900.9706	S	1.323	-0.296	1.620	932.7382	S	1.319	-0.291	1.610
901.3823	G	1.281	-0.326	1.607	932.8500	S	1.312	-0.290	1.602
901.7415	S	1.301	-0.315	1.616	933.8612	S	1.305	-0.308	1.613
901.8578	S	1.293	-0.314	1.607	933.9358	S	1.309	-0.292	1.601
902.3927	G	1.330	-0.288	1.618	934.6833	S	1.287	-0.334	1.621
902.7247	S	1.270	-0.340	1.610	934.7989	S	1.292	-0.328	1.620
902.8644	S	1.300	-0.309	1.609	934.8883	S	1.294	-0.319	1.613
902.9745	S	1.282	-0.327	1.609	935.7037	S	1.327	-0.286	1.613
903.3730	G	1.291	-0.321	1.612	935.7967	S	1.264	-0.348	1.612
903.7300	S	1.300	-0.302	1.602	936.6820	S	1.304	-0.299	1.603
903.8459	S	1.306	-0.310	1.616	936.7584	S	1.299	-0.330	1.629
904.7174	S	1.350	-0.258	1.609	940.7291	S	1.258	-0.349	1.607
904.8380	S	1.337	-0.278	1.615	940.8310	S	1.235	-0.383	1.618
904.9676	S	1.291	-0.314	1.605	943.7579	S	1.277	-0.343	1.620
905.7100	S	1.298	-0.303	1.601	944.7448	S	1.332	-0.278	1.609
905.8216	S	1.298	-0.308	1.606	944.8220	S	1.306	-0.300	1.606
906.9436	S	1.335	-0.267	1.602	945.7475	S	1.324	-0.278	1.602
907.7591	S	1.262	-0.362	1.625	945.8372	S	1.344	-0.261	1.605
907.9590	S	1.290	-0.324	1.614	946.7449	S	1.278	-0.324	1.602
908.7100	S	1.283	-0.342	1.625	946.8233	S	1.284	-0.318	1.602
908.8352	S	1.291	-0.331	1.622	947.7321	S	1.268	-0.334	1.602
908.9612	S	1.303	-0.315	1.618	947.8099	S	1.270	-0.333	1.603
911.6980	S	1.301	-0.317	1.618	948.7291	S	1.288	-0.326	1.614

Letter S marks the data from the San Pedro Martir Observatory and letter G denotes the data from the Crimean station of the GAISH.

3 INDIVIDUAL STARS

As a general reference for all programme WNL stars, we point to the study of optical emission-line strengths by Conti & Massey (1989). A summary of all available radio observations is given by Abbott et al. (1986) and Leitherer et al. (1995, 1997); infrared data are provided by Williams, van der Hucht & Thé (1987), Vreux, Andrillat & Biémont (1990), Morris et al. (1996) and Tamblyn et al. (1996). Attempts to model WNL spectra have been summarized by Crowther, Hillier & Smith (1995a,b), Crowther et al. (1995c) and Hamman, Koesterke & Wessolowski (1995).

3.1 WR 40 = HD 96548

This bright star has been observed quite extensively (Matthews & Moffat 1994; Antokhin et al. 1995, and references therein). Multiperiodic character of the variations was suggested by Balona, Egan & Marang (1989). The intricate epoch-depending light variations were decoded using two basic frequencies, $f_1 = 0.057$ and $f_2 = 0.081\ \mathrm{d}^{-1}$ along with their harmonics, and interpreted as arising from orbital motion and axial rotation of the WR component (Matthews & Moffat 1994). Based on multiple spectropolarimetric observations, Schulte-Ladbeck (1994) concludes that WR 40 has a variable wind with a time-averaged spherical geometry. Robert (1992) thoroughly discussed microvariability of the He II 5412-Å and He I 5876-Å profiles in WR 40 as caused by rapid, outward propagating wind inhomogeneities.

The time span of our observations (Fig. 2) does not allow us to sample either of the suggested periodicities. We shall discuss this star in detail below, when intercomparing the photometric and spectral variations of WR 40, 123, 124 and 156, with emphasis on the global variations of the wind structure.

3.2 WR 98 = HDE 318016

This possible long-period binary ($P = 48.7$ d, $e \sim 0$; Niemela 1991) with hybrid WN7/WC7 + ? spectrum, is known as a relatively strong non-thermal radio emitter (van der Hucht 1991). All measured C III–C IV and N IV–N V lines move in phase (Niemela 1991). We are not aware of any previous attempt to search for photometric variability of this star. We found no significant periodic variability in our 1995 data

Table 8. Photometric observations of WR 124.

HJD-2449000	Obs.	wr-c5 ΔV	wr-c3 ΔV	c5-c3 ΔV	HJD-2449000	Obs.	wr-c5 ΔV	wr-c3 ΔV	c5-c3 ΔV
519.7773	S	0.511	0.154	-0.357	906.7088	S	0.466	0.129	-0.337
520.7149	S	0.496	0.129	-0.367	907.7456	S	0.470	0.143	-0.327
521.6913	S	0.490	0.133	-0.356	907.9034	S	0.484	0.150	-0.334
522.7022	S	0.454	0.086	-0.368	908.6959	S	0.465	0.134	-0.331
523.7038	S	0.491	0.132	-0.359	908.8210	S	0.484	0.151	-0.333
524.8419	S	0.481	0.127	-0.354	908.9358	S	0.476	0.153	-0.323
525.6899	S	0.496	0.132	-0.364	909.7429	S	0.452	0.116	-0.337
525.8470	S	0.488	0.140	-0.348	909.8258	S	0.430	0.096	-0.334
526.6958	S	0.488	0.140	-0.348	909.9009	S	0.449	0.114	-0.335
526.8989	S	0.489	0.138	-0.352	910.7609	S	0.444	0.113	-0.331
527.3874	G	–	0.134	–	910.8140	S	0.453	0.129	-0.324
531.4637	G	–	0.141	–	911.7718	S	0.495	0.155	-0.340
531.4846	G	–	0.144	–	911.8760	S	0.500	0.167	-0.333
533.4063	G	0.488	0.137	-0.333	911.9476	S	0.490	0.153	-0.337
533.4294	G	0.496	0.128	-0.353	912.7926	S	0.479	0.136	-0.343
533.8828	S	0.448	0.102	-0.346	912.8808	S	0.469	0.126	-0.343
534.3927	G	0.468	0.096	-0.355	913.7938	S	0.494	0.143	-0.351
534.4151	G	0.472	0.089	-0.367	913.8874	S	0.484	0.136	-0.348
536.8393	S	0.466	0.120	-0.346	915.8411	S	0.452	0.117	-0.335
538.7576	S	0.498	0.140	-0.358	918.8411	S	0.496	0.157	-0.339
539.7791	S	0.474	0.119	-0.355	920.7685	S	0.485	0.136	-0.349
540.9358	S	0.472	0.104	-0.368	920.9483	S	0.495	0.149	-0.346
541.8654	S	0.473	0.117	-0.360	921.7301	S	0.471	0.135	-0.337
543.9100	S	0.477	0.111	-0.366	921.8753	S	0.464	0.129	-0.335
544.7838	S	0.466	0.106	-0.360	921.9621	S	0.465	0.131	-0.334
885.3865	G	0.447	0.089	-0.358	922.7663	S	0.468	0.136	-0.332
885.4857	G	0.455	0.086	-0.369	922.9026	S	0.461	0.123	-0.338
886.3695	G	0.437	0.096	-0.341	923.7504	S	0.464	0.131	-0.333
886.3793	G	0.453	0.098	-0.355	923.8565	S	0.450	0.125	-0.325
887.3361	G	0.441	0.090	-0.351	923.9174	S	0.462	0.126	-0.336
887.3580	G	0.435	0.086	-0.349	924.6892	S	0.458	0.123	-0.335
887.3655	G	0.435	0.079	-0.356	924.7621	S	0.458	0.129	-0.329
890.7478	S	0.468	0.110	-0.358	924.8932	S	0.459	0.142	-0.317
890.9664	S	0.453	0.100	-0.353	924.9596	S	0.472	0.148	-0.324
891.7119	S	0.437	0.105	-0.332	925.6928	S	0.494	0.170	-0.324
891.9486	S	0.454	0.100	-0.354	925.7640	S	0.502	0.176	-0.326
892.3309	G	0.458	0.117	-0.341	925.8812	S	0.494	0.158	-0.336
892.3391	G	0.442	0.101	-0.341	926.6930	S	0.467	0.132	-0.335
892.4444	G	0.475	0.123	-0.352	926.7737	S	0.451	0.117	-0.334
892.7612	S	0.424	0.098	-0.326	927.7509	S	0.445	0.111	-0.334
893.3301	G	0.481	0.132	-0.349	928.6904	S	0.470	0.136	-0.334
893.3374	G	0.481	0.141	-0.340	928.8204	S	0.474	0.132	-0.341
893.4558	G	0.476	0.112	-0.364	929.6899	S	0.474	0.136	-0.338
893.8759	S	0.450	0.118	-0.332	929.7723	S	0.470	0.132	-0.338
894.3320	G	0.470	0.136	-0.334	929.8759	S	0.484	0.138	-0.346
894.3391	G	0.456	0.128	-0.328	930.6863	S	0.458	0.120	-0.338
894.7918	S	0.493	0.150	-0.343	930.7708	S	0.457	0.114	-0.343
894.9244	S	0.490	0.147	-0.343	930.8699	S	0.457	0.112	-0.345
895.3444	G	0.453	0.115	-0.338	931.6864	S	0.460	0.116	-0.344
895.3515	G	0.459	0.126	-0.333	931.7688	S	0.466	0.120	-0.346
895.7733	S	0.476	0.133	-0.343	931.8806	S	0.447	0.117	-0.330
897.3365	G	0.466	0.135	-0.331	932.7506	S	0.474	0.133	-0.341
897.3432	G	0.462	0.127	-0.335	932.8617	S	0.449	0.099	-0.350
897.4583	G	0.451	0.104	-0.347	933.8732	S	0.480	0.146	-0.334
897.7339	S	0.464	0.140	-0.324	933.9487	S	0.485	0.144	-0.341
897.9265	S	0.452	0.114	-0.338	934.6952	S	0.443	0.096	-0.347
898.6930	S	0.463	0.120	-0.343	934.8141	S	0.445	0.101	-0.344
898.8414	S	0.440	0.110	-0.330	934.9001	S	0.451	0.108	-0.343
899.6898	S	0.484	0.141	-0.343	935.7160	S	0.457	0.114	-0.343
899.8481	S	0.479	0.133	-0.346	935.8092	S	0.452	0.116	-0.336
899.9533	S	0.466	0.120	-0.346	935.9346	S	0.470	0.130	-0.341
900.6900	S	0.468	0.119	-0.349	936.6950	S	0.456	0.118	-0.337
900.8483	S	0.466	0.113	-0.353	936.7711	S	0.451	0.116	-0.335
901.3335	G	0.446	0.098	-0.348	937.7112	S	0.463	0.122	-0.341
901.3389	G	0.462	0.095	-0.367	937.7966	S	0.453	0.127	-0.326
901.4547	G	0.458	0.089	-0.369	937.8761	S	0.446	0.126	-0.320
901.7107	S	0.470	0.116	-0.354	938.7447	S	0.448	0.120	-0.329
901.8435	S	0.467	0.110	-0.357	938.8349	S	0.457	0.128	-0.332
902.4237	G	0.452	0.107	-0.345	940.7489	S	0.465	0.126	-0.339
902.4295	G	0.447	0.099	-0.348	940.8508	S	0.475	0.117	-0.358
902.7065	S	0.478	0.122	-0.353	941.7772	S	0.465	0.116	-0.349
902.8487	S	0.481	0.128	-0.353	941.8584	S	0.457	0.117	-0.340
903.3049	G	0.501	0.163	-0.338	943.7740	S	0.476	0.137	-0.339
903.3109	G	0.492	0.157	-0.335	944.7583	S	0.448	0.108	-0.340
903.4336	G	0.486	0.148	-0.338	944.8389	S	0.454	0.116	-0.338
903.4391	G	0.495	0.141	-0.354	945.7616	S	0.484	0.133	-0.352
903.7173	S	0.487	0.143	-0.344	945.8520	S	0.462	0.119	-0.343
903.9488	S	0.476	0.134	-0.342	946.7598	S	0.478	0.123	-0.355
904.7046	S	0.467	0.124	-0.343	946.8396	S	0.466	0.120	-0.346
904.8189	S	0.488	0.135	-0.353	947.7450	S	0.488	0.134	-0.354
904.9542	S	0.462	0.120	-0.342	948.7441	S	0.449	0.104	-0.345
905.6974	S	0.426	0.106	-0.320					
905.8020	S	0.447	0.108	-0.339					

Letter S marks the data from the San Pedro Martir Observatory and letter G denotes the data from the Crimean station of the GAISH.

Table 9. Photometric observations of WR 130.

HJD-2449000	Obs.	wr-c3 ΔV	wr-c2 ΔV	c2-c3 ΔV	HJD-2449000	Obs.	wr-c3 ΔV	wr-c2 ΔV	c2-c3 ΔV
519.9768	S	1.262	1.657	-0.395	901.4678	G	1.277	1.659	-0.381
521.7711	S	1.273	1.669	-0.396	901.7551	S	1.256	1.648	-0.392
522.7782	S	1.273	1.656	-0.383	901.8934	S	1.276	1.659	-0.383
524.8163	S	1.266	1.642	-0.376	902.4638	G	1.298	1.680	-0.381
525.7537	S	1.240	1.625	-0.385	902.4692	G	1.306	1.687	-0.380
525.8486	S	1.254	1.638	-0.384	902.7940	S	–	1.669	–
526.4659	G	1.231	1.619	-0.387	902.9600	S	1.287	1.678	-0.391
526.7778	S	1.226	1.616	-0.390	903.4499	G	1.272	1.650	-0.377
527.3635	G	1.246	1.608	-0.362	903.4550	G	1.303	1.701	-0.397
527.4632	G	1.276	1.658	-0.382	903.4745	G	1.272	1.659	-0.386
527.8588	S	1.261	1.647	-0.386	903.4795	G	1.283	1.662	-0.378
528.6908	S	1.241	1.626	-0.385	903.8194	S	1.284	1.663	-0.379
531.4951	G	1.289	1.695	-0.405	903.9611	S	1.271	1.651	-0.380
531.5176	G	1.289	1.680	-0.390	904.7448	S	1.284	1.671	-0.387
531.8773	S	1.272	1.662	-0.390	904.9367	S	1.262	1.648	-0.386
533.3561	G	1.226	1.623	-0.396	905.7685	S	1.269	1.640	-0.371
533.3784	G	1.244	1.637	-0.392	906.9554	S	1.318	1.699	-0.381
533.7135	S	1.240	1.632	-0.392	907.8430	S	1.282	1.657	-0.375
533.9499	S	1.261	1.650	-0.389	907.9680	S	–	1.662	–
534.3408	G	1.259	1.630	-0.370	908.7969	S	1.268	1.651	-0.383
534.3637	G	1.247	1.653	-0.405	908.9084	S	1.264	1.648	-0.384
536.7039	S	1.276	1.657	-0.381	909.7619	S	1.254	1.638	-0.384
536.8635	S	1.294	1.690	-0.396	909.8426	S	1.262	1.651	-0.389
537.7286	S	1.272	1.666	-0.395	909.9152	S	1.261	1.627	-0.366
537.8329	S	1.273	1.667	-0.394	910.7758	S	1.262	1.648	-0.386
538.6968	S	1.273	1.662	-0.389	911.7971	S	1.290	1.672	-0.382
538.9098	S	1.288	1.674	-0.383	911.9024	S	1.272	1.656	-0.384
539.7324	S	1.274	1.660	-0.386	912.8080	S	–	1.642	–
539.8490	S	1.268	1.644	-0.376	913.8104	S	–	1.670	–
540.8358	S	1.256	1.648	-0.392	915.8579	S	1.294	1.685	-0.391
540.9669	S	1.258	1.645	-0.387	920.8178	S	1.263	1.638	-0.375
541.7490	S	1.244	1.642	-0.398	920.9646	S	1.285	1.656	-0.371
541.8470	S	1.261	1.647	-0.386	921.7448	S	1.303	1.678	-0.375
542.7445	S	1.250	1.656	-0.406	921.8958	S	1.296	1.674	-0.378
543.8186	S	1.248	1.643	-0.395	922.9191	S	1.297	1.660	-0.363
543.9425	S	1.240	1.632	-0.392	923.7646	S	1.294	1.676	-0.381
544.8022	S	1.260	1.661	-0.400	924.7748	S	1.278	1.667	-0.389
885.3481	G	1.249	1.623	-0.373	924.9054	S	1.270	1.656	-0.387
885.5146	G	1.262	1.646	-0.380	924.9723	S	1.278	1.657	-0.379
886.3500	G	1.296	1.644	-0.348	925.7847	S	1.260	1.644	-0.384
886.3907	G	1.285	1.672	-0.385	925.9044	S	1.254	1.637	-0.383
887.3235	G	1.263	1.628	-0.364	926.7853	S	1.270	1.652	-0.382
887.3454	G	1.257	1.638	-0.380	928.7853	S	1.295	1.667	-0.372
887.4006	G	1.275	1.648	-0.372	928.8897	S	1.294	1.667	-0.373
890.7964	S	1.295	1.664	-0.369	929.7838	S	1.287	1.671	-0.384
891.3068	G	1.280	1.690	-0.409	929.8872	S	1.271	1.664	-0.393
891.9302	S	1.271	1.645	-0.374	930.7815	S	1.271	1.654	-0.383
892.3086	G	1.274	1.628	-0.390	930.8808	S	1.276	1.654	-0.378
892.3174	G	1.236	1.621	-0.383	931.8021	S	1.263	1.646	-0.383
892.4640	G	1.266	1.641	-0.374	932.8286	S	1.269	1.661	-0.392
892.8893	S	1.266	1.654	-0.388	933.9100	S	–	1.646	–
893.3112	G	1.272	1.655	-0.382	933.9688	S	1.252	1.639	-0.387
893.3183	G	1.265	1.641	-0.376	934.7728	S	1.266	1.634	-0.368
893.4649	G	1.272	1.650	-0.377	934.8630	S	1.266	1.648	-0.382
893.8575	S	1.282	1.663	-0.381	935.7630	S	1.271	1.641	-0.370
894.3096	G	1.265	1.667	-0.400	935.8601	S	1.263	1.636	-0.373
894.3158	G	1.297	1.660	-0.362	936.7314	S	1.274	1.672	-0.398
894.8339	S	1.271	1.645	-0.374	936.8058	S	1.275	1.657	-0.382
894.9511	S	1.276	1.648	-0.372	937.7272	S	1.240	1.630	-0.390
895.8106	S	1.260	1.647	-0.387	937.8086	S	1.282	1.656	-0.375
897.4677	G	1.253	1.626	-0.372	937.8878	S	1.278	1.658	-0.380
897.4737	G	1.253	1.628	-0.374	938.7664	S	1.249	1.622	-0.373
897.8577	S	1.277	1.654	-0.377	940.7702	S	1.266	1.658	-0.392
897.9575	S	1.279	1.667	-0.388	941.7964	S	1.286	1.659	-0.373
898.7684	S	1.285	1.660	-0.375	944.7734	S	1.310	1.687	-0.377
899.8110	S	1.271	1.656	-0.385	945.7807	S	1.254	1.649	-0.395
899.9352	S	1.266	1.652	-0.386	946.7748	S	–	1.670	–
900.8059	S	1.283	1.667	-0.384	947.7604	S	1.281	1.671	-0.390
900.9487	S	1.258	1.651	-0.393	948.7584	S	–	1.670	–
901.4626	G	1.262	1.641	-0.378					

Letter S marks the data from the San Pedro Martir Observatory and letter G denotes the data from the Crimean station of the GAISH.

(Fig. 3), despite the large amplitude of the light variations. There is no obvious relation of these fluctuations to the binary phase.

3.3 WR 105 = NS 4 = AS 268 = Ve 2-47

Recently, this star was reclassified by Smith et al. (1996) as WN9h. Nothing was known previously about the temporal behaviour of this star. There are two possible periodicities in our CLEANed (Roberts, Lehar & Dreher 1987; cf. Antokhin et al. 1995) power spectrum (PS): $f_1 = 0.760 \pm 0.002$ and $f_2 = 1.244 \pm 0.002\ \mathrm{d}^{-1}$ ($\pm$FWHM of the typical unblended peaks in the original PS). They are obviously related by 1-d aliases to the fundamental harmonics $f_3 = 0.242\ \mathrm{d}^{-1}$, seen in the *original* PS and corresponding to a feature with peak-to-valley amplitude $A = 0.019$ mag. This is a good example demonstrating that the results of CLEANing cannot be taken at face value. The false-alarm probability (Scargle

Table 10. Photometric observations of WR 148 in 1995.

HJD-2449000	Obs.	wr-c3 ΔV	wr-c2 ΔV	c2-c3 ΔV	HJD-2449000	Obs.	wr-c3 ΔV	wr-c2 ΔV	c2-c3 ΔV
885.5005	G	0.087	0.003	0.084	922.7975	S	0.071	-0.011	0.082
886.5122	G	0.072	-0.018	0.089	923.7742	S	0.090	-0.004	0.094
890.8068	S	0.063	-0.024	0.087	924.7846	S	0.077	-0.009	0.086
891.8843	S	0.058	-0.032	0.091	924.9160	S	0.076	-0.011	0.087
892.4847	G	0.053	-0.035	0.088	924.9810	S	0.084	-0.009	0.093
893.4893	G	0.079	-0.008	0.086	925.7987	S	0.086	-0.012	0.098
893.8890	S	0.092	0.006	0.086	925.9134	S	0.073	-0.013	0.086
894.8766	S	0.093	-0.003	0.096	926.7993	S	0.077	-0.012	0.089
895.8314	S	0.081	-0.004	0.085	928.7968	S	0.084	-0.004	0.088
897.4924	G	0.100	0.006	0.094	928.9001	S	0.080	-0.008	0.088
897.8806	S	0.096	0.011	0.085	929.7929	S	0.065	-0.030	0.095
898.8166	S	0.087	0.001	0.086	929.8966	S	0.063	-0.029	0.092
899.8232	S	0.079	-0.012	0.091	930.7904	S	0.056	-0.032	0.088
900.8168	S	0.076	-0.014	0.090	930.8907	S	0.070	-0.023	0.093
901.4872	G	0.102	0.008	0.094	931.8105	S	0.088	-0.006	0.094
901.8058	S	0.074	-0.014	0.088	931.9010	S	0.090	-0.003	0.093
901.9338	S	0.080	-0.007	0.087	932.8388	S	0.092	-0.001	0.093
902.4944	G	0.090	0.012	0.077	933.9185	S	0.071	-0.019	0.090
902.8248	S	0.106	0.019	0.087	933.9773	S	0.074	-0.013	0.087
903.4936	G	0.109	0.021	0.088	934.7817	S	0.073	-0.017	0.090
903.9211	S	0.105	0.016	0.089	934.8716	S	0.080	-0.006	0.086
904.9010	S	0.111	0.019	0.092	935.7725	S	0.074	-0.016	0.090
905.8837	S	0.094	-0.001	0.095	936.7393	S	0.083	-0.011	0.094
907.8616	S	0.083	-0.008	0.091	936.8136	S	0.086	-0.001	0.087
908.8907	S	0.071	-0.015	0.086	937.7340	S	0.089	0.002	0.087
909.7747	S	0.081	-0.014	0.095	937.8180	S	0.093	0.011	0.082
909.8561	S	0.086	-0.005	0.091	937.8983	S	0.091	0.003	0.088
909.9278	S	0.087	-0.004	0.091	938.7758	S	0.083	-0.010	0.093
910.7915	S	0.092	0.003	0.089	938.8695	S	0.080	-0.016	0.096
911.8321	S	0.095	0.003	0.092	940.7857	S	0.084	-0.009	0.093
912.8223	S	0.077	-0.014	0.091	941.8161	S	0.073	-0.016	0.089
913.8259	S	0.071	-0.018	0.089	944.8529	S	0.074	-0.016	0.090
920.8675	S	0.076	-0.012	0.088	945.8530	S	0.082	-0.008	0.090
920.9773	S	0.070	-0.019	0.089	946.8534	S	0.069	-0.015	0.084
921.7560	S	0.082	-0.010	0.092	948.7702	S	0.064	-0.028	0.092
921.9108	S	0.086	-0.006	0.092					

Letter S marks the data from the San Pedro Martir Observatory and letter G denotes the data from the Crimean station of the GAISH.

1982) of the $f_3=0.242\,d^{-1}$ feature is only $p=0.19$, which is too high a value for f_3 to be considered as significant: $p \lesssim 0.001$ can be regarded as necessary for a statistically significant periodicity in a relatively small, $N \leq 100$, data set. There are at least two possibilities for diminishing the significance of the $f_3=0.242\,d^{-1}$ frequency: (1) either f_3 is not stable during the observations, or (2) f_3 is effectively masked by intrinsic 'flicker', i.e., random (or short-lived) intrinsic variations (Fig. 4). The latter seems to be a common cause of variability in practically all observed WN8 stars.

3.4 WR 116 = ST 1 = AS 306

Nothing was known previously about the optical variability of this star. We found one of our comparison stars, c2, to be variable with $f=0.371 \pm 0.001\,d^{-1}$; we removed appropriate least-squares-fitted sine-wave at this frequency from all wr-c2 and c2-c3 data (Fig. 5). In our CLEANed 1994–1995 data we detect periodicity with $f=0.173 \pm 0.002\,d^{-1}$ and $A=0.043$ mag (Fig. 5) plus at least two higher harmonics. The false-alarm probability is fairly low: $p=0.002$.

3.5 WR 120 = Vy 1-3

This previously unobserved star demonstrates the highest level of activity among all WNL stars. The best periodicity derived from our 1995 photometry (Fig. 6) has $f=0.145 \pm 0.018\,d^{-1}$, $A=0.043$ mag and $p=0.060$, which is not low enough to consider this period as significant. It is

Table 11. Photometric observations of WR 156.

HJD-2449000	Obs.	wr-c2 ΔV	wr-c3 ΔV	c3-c2 ΔV	HJD-2449000	Obs.	wr-c2 ΔV	wr-c3 ΔV	c3-c2 ΔV
522.9625	S	1.264	–	–	921.9736	S	1.321	1.002	0.319
524.9233	S	1.275	–	–	922.8069	S	1.313	1.000	0.313
525.8660	S	1.278	0.970	0.308	922.9307	S	1.308	0.996	0.312
526.8598	S	1.273	0.979	0.294	923.7893	S	1.338	1.026	0.312
526.9526	S	1.279	0.978	0.301	924.8124	S	1.342	1.028	0.314
533.9296	S	1.267	0.969	0.298	924.8753	S	1.342	1.038	0.304
536.8788	S	1.322	1.026	0.296	924.9327	S	1.335	1.025	0.310
537.8921	S	1.292	0.990	0.302	924.9881	S	1.338	1.026	0.312
538.8848	S	1.266	0.954	0.312	925.7712	S	1.316	1.013	0.303
540.9465	S	1.274	0.974	0.300	925.8908	S	1.319	1.007	0.312
541.9070	S	1.296	0.996	0.300	925.9329	S	1.314	1.004	0.310
543.9214	S	1.273	0.978	0.295	926.7488	S	1.318	1.009	0.309
544.8291	S	1.299	1.003	0.296	926.8790	S	1.316	1.007	0.309
886.5246	G	1.292	0.990	0.320	928.7493	S	1.311	1.001	0.310
890.9439	S	1.310	0.997	0.313	928.8340	S	1.305	0.994	0.311
891.9078	S	1.328	1.006	0.322	929.7401	S	1.306	1.002	0.304
892.5160	G	1.324	1.011	0.310	929.8405	S	1.321	1.005	0.316
892.9367	S	1.326	1.009	0.317	929.9108	S	1.314	1.006	0.308
893.5068	G	1.312	1.003	0.313	930.7382	S	1.315	1.011	0.304
893.9006	S	1.318	1.002	0.316	930.8352	S	1.311	0.998	0.313
894.8888	S	1.301	1.001	0.300	930.9042	S	1.313	1.004	0.309
894.9619	S	1.311	1.002	0.309	931.7380	S	1.312	1.004	0.308
895.8431	S	1.314	1.015	0.299	931.8565	S	1.317	1.000	0.317
897.5050	G	1.316	1.005	0.310	931.9272	S	1.317	1.006	0.311
897.8954	S	1.338	1.032	0.306	932.7587	S	1.310	1.002	0.308
898.8981	S	1.325	1.015	0.310	932.8687	S	1.319	1.003	0.316
899.9062	S	1.278	0.962	0.316	933.8808	S	1.325	1.014	0.311
900.9324	S	1.304	0.992	0.312	933.9561	S	1.319	1.011	0.308
901.5086	G	1.322	1.011	0.310	934.7046	S	1.307	1.000	0.307
901.9192	S	1.309	0.999	0.310	934.8215	S	1.306	0.994	0.312
902.5072	G	1.292	0.982	0.312	934.9077	S	1.312	0.996	0.316
902.9362	S	1.321	1.011	0.310	935.7239	S	1.320	1.011	0.309
903.5060	G	1.323	1.009	0.305	935.8351	S	1.331	1.023	0.308
903.9291	S	1.323	1.009	0.314	935.9192	S	1.334	1.023	0.311
904.9220	S	1.311	1.000	0.311	936.7041	S	1.341	1.030	0.311
905.9045	S	1.317	1.005	0.312	936.7800	S	1.332	1.029	0.303
906.9643	S	1.330	1.021	0.309	937.7420	S	1.339	1.029	0.310
907.8708	S	1.298	0.989	0.309	937.8254	S	1.322	1.014	0.308
908.9432	S	1.313	0.998	0.315	937.9065	S	1.341	1.034	0.307
909.7849	S	1.292	0.985	0.307	938.7527	S	1.326	1.013	0.313
909.8649	S	1.301	0.987	0.314	938.8438	S	1.316	1.005	0.311
910.8004	S	1.326	1.008	0.318	940.8001	S	1.327	1.018	0.309
911.8432	S	1.319	1.009	0.310	940.8658	S	1.320	1.017	0.303
911.9144	S	1.320	1.016	0.304	941.8293	S	1.314	0.999	0.315
912.8325	S	1.311	1.002	0.309	941.8716	S	1.317	1.007	0.310
912.8919	S	1.310	0.999	0.311	944.7841	S	1.295	0.982	0.313
913.8367	S	1.319	1.012	0.307	944.8637	S	1.296	0.984	0.312
913.8964	S	1.318	1.011	0.307	945.7908	S	1.285	0.984	0.301
915.9019	S	1.314	1.006	0.308	946.7855	S	1.302	0.991	0.311
920.7810	S	1.339	1.032	0.307	946.8634	S	1.291	0.988	0.303
920.9888	S	1.336	1.022	0.314	947.7698	S	1.311	1.004	0.307
921.7694	S	1.321	1.001	0.320	948.7801	S	1.322	1.015	0.307
921.9226	S	1.314	1.004	0.310					

Letter S marks the data from the San Pedro Martir Observatory and letter G denotes the data from the Crimean station of the GAISH.

Table 12. Spectroscopic observations of WR 123.

HJD-2449000	Obs.	RV km s^{-1}	$\sigma(RV)$ km s^{-1}	HJD-2449000	Obs.	RV km s^{-1}	$\sigma(RV)$ km s^{-1}
857.835	M	–	33.6(!)	941.792	D	-12.3	2.8
932.677	M	12.5	7.5	942.849	D	7.9	4.3
936.623	M	-8.1	6.6	943.727	D	0.5	3.1
936.763	M	-14.1	9.3	969.588	M	–	26.7
937.630	M	-11.6	2.8	992.599	M	21.9	8.2
937.767	M	-20.7	11.3	993.527	M	38.0	22.0
938.615	M	-7.1	3.0	999.674	D	-19.9	13.4
938.759	M	-35.9	10.8	1001.524	M	25.9	11.1
939.628	M	-7.2	3.5	1002.524	M	21.3	5.9
939.772	M	-21.5	9.0	1002.644	D	-9.5	12.6
940.612	M	3.3	2.4	1003.512	M	19.0	10.0
940.748	M	-10.5	5.9	1004.504	M	2.0	5.4
940.823	D	4.1	13.5	1004.659	D	14.1	12.0

Letter M marks the data from the Mont Mégantic Observatory, and letter D denotes the data from the Dominion Astrophysical Observatory.

Table 13. Spectroscopic observations of WR 124.

HJD-2449000	Obs.	RV km s^{-1}	$\sigma(RV)$ km s^{-1}	HJD-2449000	Obs.	RV km s^{-1}	$\sigma(RV)$ km s^{-1}
857.769	M	–	–	941.740	D	-10.3	2.7
860.769	M	13.5	8.6	941.851	D	-8.0	1.7
884.709	M	-3.6	2.7	942.788	D	-15.0	2.7
888.792	M	-7.0	3.5	942.898	D	0.3	3.1
889.640	M	2.0	2.0	943.765	D	-22.7	4.0
890.650	M	13.3	6.0	943.882	D	-9.7	4.4
936.678	M	2.6	5.6	967.701	M	16.7	12.8
936.839	M	12.6	7.2	971.596	M	17.5	8.3
937.681	M	-13.1	9.1	992.553	M	13.1	5.4
937.826	M	2.2	7.9	993.608	M	15.2	8.5
938.666	M	-4.6	1.0	999.642	D	-11.6	3.4
938.819	M	-19.2	6.8	1001.585	M	0.4	2.0
939.684	M	-5.8	5.6	1002.591	M	20.9	8.3
939.827	M	-23.5	12.2	1002.708	D	-3.6	7.3
940.662	M	-24.8	12.3	1003.574	M	12.6	6.2
940.804	M	-2.4	2.7	1003.684	D	10.9	4.5
940.885	D	-3.6	8.8	1004.568	M	5.2	4.0
941.729	M	-9.1	5.2	1004.728	D	6.6	2.2

Letter M marks the data from the Mont Mégantic Observatory, and letter D denotes the data from the Dominion Astrophysical Observatory.

Table 14. Spectroscopic observations of WR 156.

HJD-2449000	Obs.	RV km s^{-1}	$\sigma(RV)$ km s^{-1}	HJD-2449000	Obs.	RV km s^{-1}	$\sigma(RV)$ km s^{-1}
889.750	M	7.4	3.0	943.932	D	-2.5	3.5
890.768	M	21.2	8.6	969.735	M	8.3	4.2
936.720	M	-17.2	1.2	970.769	M	-6.9	2.6
936.872	M	5.1	3.6	971.799	M	-13.9	5.7
937.707	M	-10.1	2.2	992.657	M	12.9	4.5
937.873	M	-10.4	2.9	992.813	M	9.0	1.6
938.715	M	1.8	3.6	995.888	M	4.3	2.7
938.851	M	-17.4	7.9	1001.754	M	-6.9	3.8
939.721	M	6.4	4.5	1002.815	M	8.4	3.5
939.860	M	1.8	2.4	1002.828	D	-2.1	2.7
940.705	M	2.4	2.8	1002.934	D	-3.2	3.3
940.842	M	-12.1	7.2	1003.721	M	7.8	3.9
940.944	D	-15.9	5.7	1004.836	M	7.0	2.6
941.937	D	-5.7	3.3	1004.872	D	4.0	3.8
942.957	D	-16.6	3.1				

Letter M marks the data from the Mont Mégantic Observatory, and letter D denotes the data from the Dominion Astrophysical Observatory.

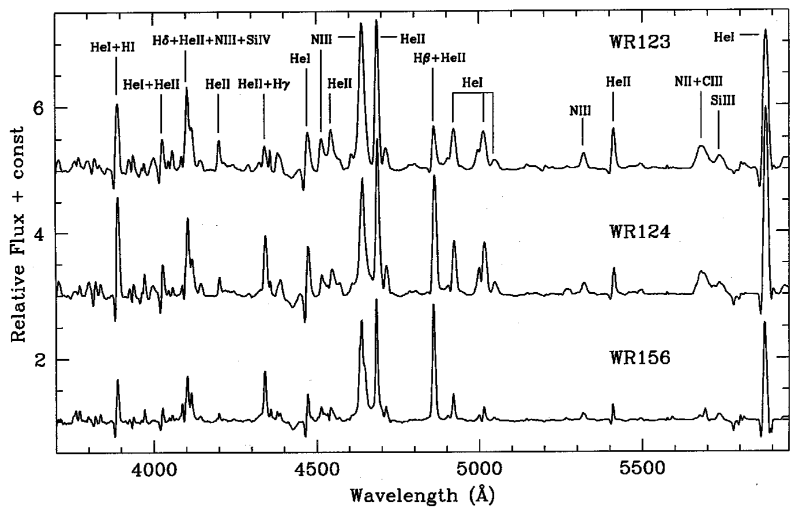

Figure 1. Mean spectra of WR 123, 124 and 156 from our 1995 observations.

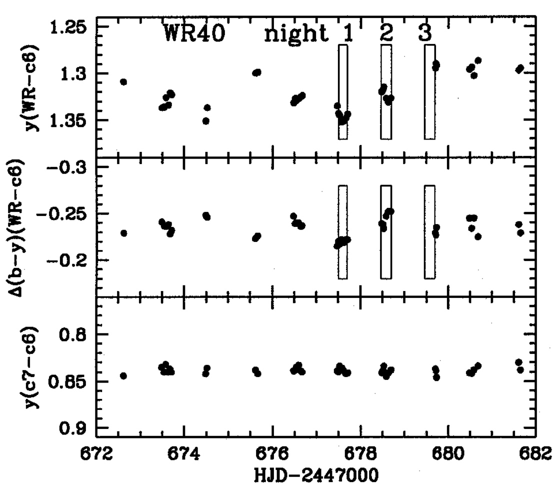

Figure 2. Strömgren b, y photometry ($\sim$continuum) of WR 40 in 1989. Thin-line boxes denote the times during which high-resolution spectra were obtained.

obvious that WR 120 is also variable on a $\sim$monthly basis, but the data are insufficient for any quantitative implications.

3.6 WR 123 = HD 177230

This star has abundant photometry (Moffat & Shara 1986; Antokhin 1987; Antokhin & Cherepashchuk 1989; van Genderen et al. 1991) with different suggested (multi)periodicities: f=0.169, 0.215 and 0.290 d^{-1} (Antokhin & Cherepashchuk 1989); f=0.422 d^{-1} with aliases f_a=0.571 and 1.428 d^{-1} (Moffat & Shara 1986). Contradicting the results of Moffat & Shara, van Genderen et al. (1991) reported a peculiar light curve with f=0.515 d^{-1}, two unequal maxima and strong colour variations. Despite the remarkable level of $\sim$periodic photometric activity, polarimetry of WR 123 does not show any coherent behaviour (St-Louis et al. 1988). However, the polarimetric data are too sparse for adequate sampling of the day-to-week variations

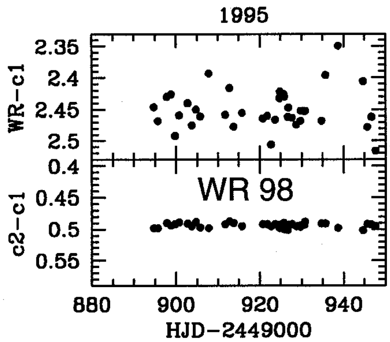

Figure 3. Broad-band (Johnson *V*) photometry of WR 98 in 1995.

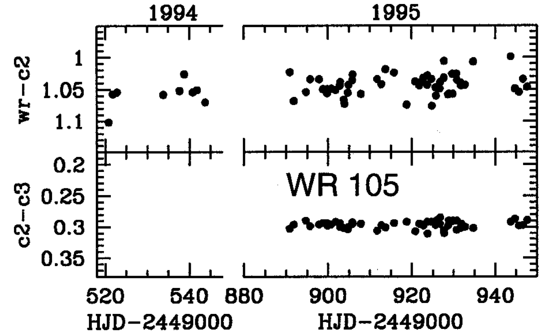

Figure 4. Broad-band (Johnson *V*) photometry of WR 105 in 1994–1995.

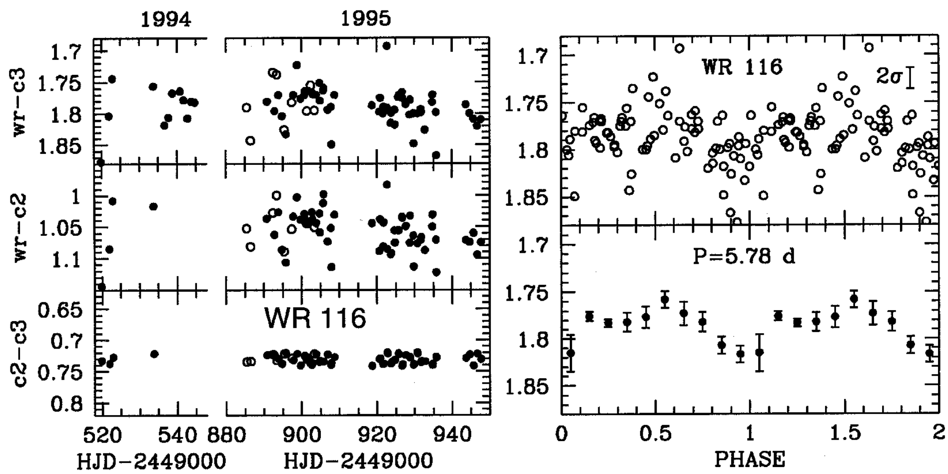

Figure 5. Left-hand panel: broad-band (Johnson *V*) photometry of WR 116 in 1994–1995. Right-hand panel: the light curve folded with $P=5.78$ d. Open circles in the left-hand panel denote the data obtained at Crimea (Ukraine), and filled circles correspond to the San Pedro Martir (Mexico) observatons.

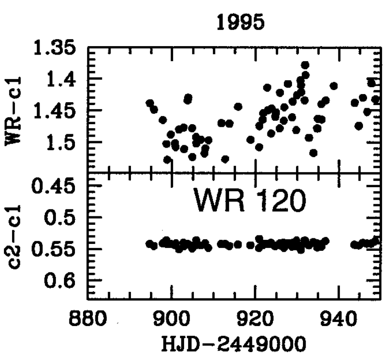

Figure 6. The same as Fig. 4, but for WR 120 in 1995.

emerging from the photometry. The search for periodic radial velocity variations puts a stringent limit on any potential change as being due to orbital motion in a binary: $K \leq 20$ km s^{-1} (Massey & Conti 1980). Later, with new data, this conclusion was questioned by Lamontagne et al. (1983), who discovered small-amplitude ($K=17$–22 km s^{-2}) periodic ($f=0.5677$ d^{-1}, or $\sim$1-d alias at $f=0.4351$ d^{-1}) variations in spectral lines, and the star was classified as a WR + c candidate (WR star and compact companion: a neutron star or a black hole).

Our 1994–1995 photometry (Fig. 7) confirms the very high level of activity indicated by all previous observations. Analysis of the original and CLEANed PS helps to pre-select six features at $f_1=0.295$ ($A=0.028$), $f_2=0.338$ ($A=0.026$), $f_3=0.578$ ($A=0.014$), $f_4=0.609$ ($A=0.027$), $f_5=0.870$ ($A=0.017$) and $f_6=1.394$ ($A=0.029$), all with ± 0.002 d^{-1}. The peak-to-valley amplitudes were evaluated by simultaneous least-squares fitting of six sinusoids with all the f_1–f_6 frequencies to the original data using the PERDET code (Breger 1989). Within the uncertainties, f_3 and f_5 may be interpreted as higher harmonics of f_1. Note that $f_1=0.295$ and $f_3=0.578$ are very close to $f=0.290$ d^{-1} (Antokhin & Cherepashchuk 1989) and $f=0.571$ d^{-1} (Moffat & Shara 1986). In an attempt to restore the shape of the light curve, we overplot in Fig. 7 the sum of the fitted f_1–f_6 frequencies. However, the success of the restoration is limited: about 50 per cent of the power still 'escapes', causing random fluctuations around the modelled light curve. This might be partially explained by taking into account the probable instability of some 'basic' PS components (Marchenko & Moffat 1997). In this star, as well as for WR 124 (two frequencies; see below), we derive false-alarm probabilities

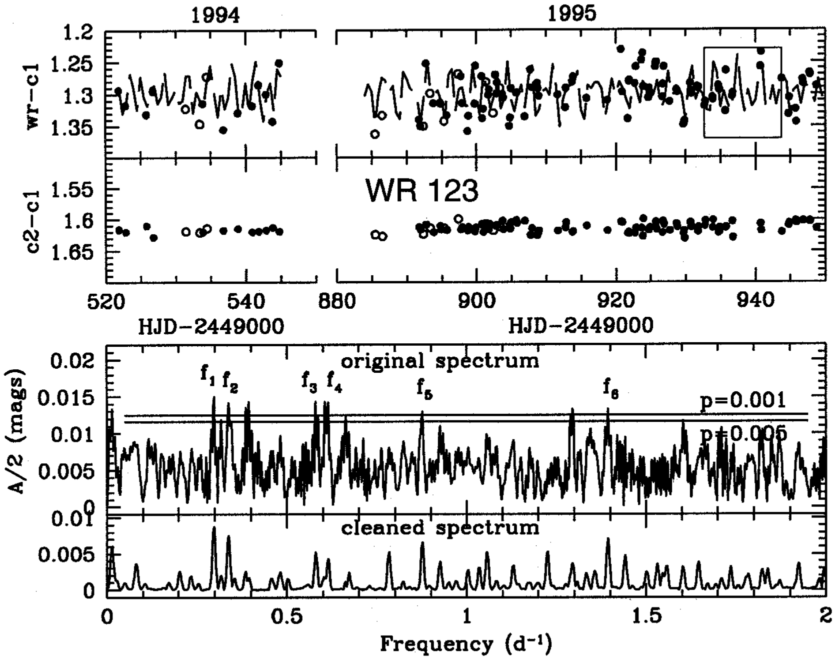

Figure 7. Upper panel: broad-band (V) photometry of WR 123 in 1994–1995. The dashed line is the sum of six sinusoids (see text). Open circles denote the data obtained at Crimea (Ukraine). Filled circles correspond to the San Pedro Martir (Mexico) observations. The box defines the dates of simultaneous spectroscopy. Bottom panel: the original frequency spectrum with $p=0.001$ and 0.005 false-alarm probability thresholds, and cleaned frequency spectrum.

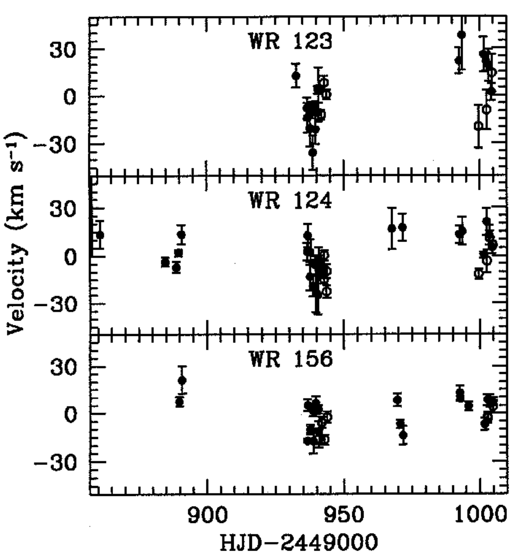

Figure 8. Radial velocities for WR 123, 124 and 156 from 1995 observations. Open circles correspond to DAO observations, and filled circles denote the MMO observations.

using the estimation of the rms amplitudes *after* subtraction of the frequencies f_1–f_6. For the rest of the stars we boldly apply the initial, assumption-free rms amplitudes.

In complete accordance with the photometry, our 1995 spectroscopy reveals the highest level of activity among the three simultaneously observed stars (WR 123, 124 and 156). Contrary to all expectations, a search for periodic variations in radial velocities brings no significant results. All available measurements are plotted in Fig. 8. The scatter of the measured RVs, $\sigma(RV)=17.8$ km s^{-1}, allows one to put an upper limit on the RV amplitude arising from hypothetical binary motion of the WR component: $K\leq 25$ km s^{-1}, in complete accordance with the value derived by Massey & Conti (1980). We shall discuss causal relationships between photometric and spectral variations in WR 123 later in Section 4.

3.7 WR 124 = 209 BAC

This star is surrounded by a spectacular ring (or planetary?) nebula M1-67, whose status is the subject of a long-lasting debate (cf. Crawford & Barlow 1991; Nota 1995, and references therein). In the heat of the debate about the Population I or PN origin of the nebula, the central star was listed as [WN8]?(SB1) (van der Hucht et al. 1988) – with the remarkably high spatial velocity of $\gtrsim 200$ km s^{-1}. Not surprisingly, WR 124 was suspected to be a runaway massive binary with a compact companion and 2.36-d (or 1.74-d alias) orbital period, deduced from the radial velocity and light variations (Moffat, Lamontagne & Seggewiss 1982). A slightly different period of 2.73 d plus significant scatter around the 'phased' light curve was found by Moffat & Shara (1986) in broad-band B observations. A series of polarimetric observations over 8 d (St-Louis et al. 1988) showed only incoherent variations.

We found the comparison star c3 to be variable and removed the periodic component with $f=0.069\,\mathrm{d}^{-1}$ from the wr-c3 and c5-c3 light curves. In so doing, the aperiodic component of the variability of c3 remained unaffected. We note the relatively low level activity of WR 124, both photometric (Fig. 9) and spectral (see below). The CLEANED PS reveals two possible periods: $f_1=0.225$ and

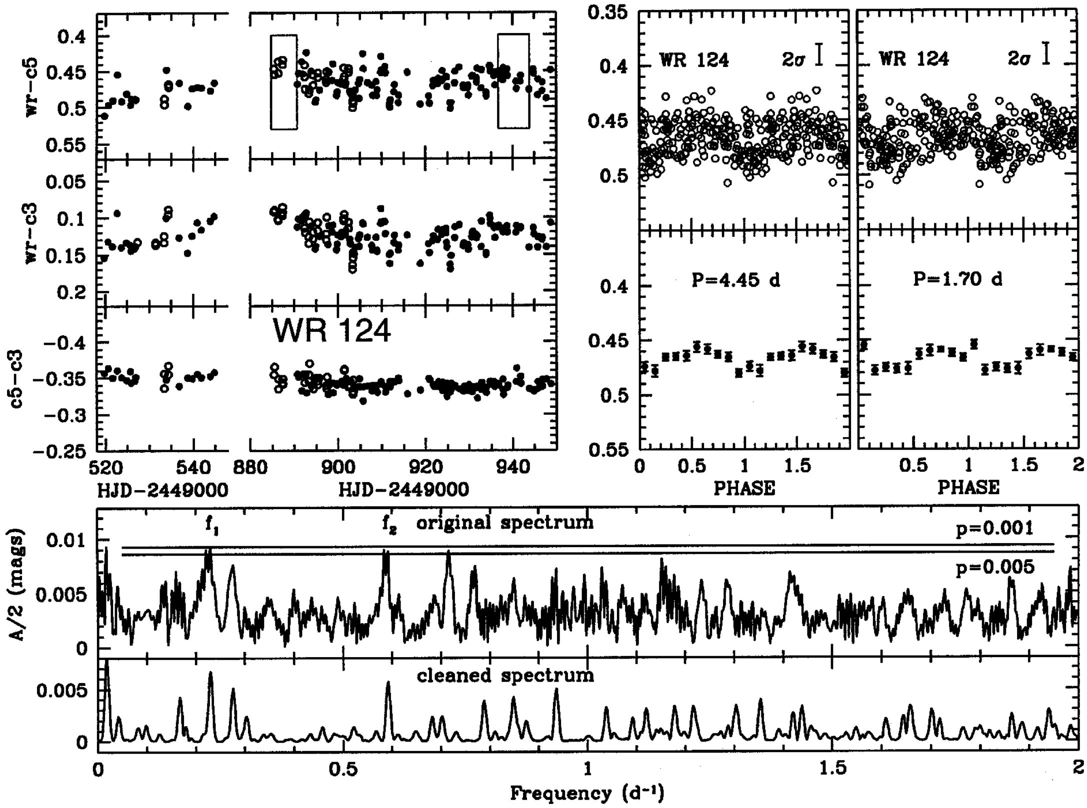

Figure 9. Left upper panel: broad-band (V) photometry of WR 124 in 1994–1995. Open dots mark the data obtained at Crimea (Ukraine). Filled dots correspond to the San Pedro Martir (Mexico) observations. The thin-line boxes define the dates of simultaneous spectroscopy. Right upper panel: the light curves folded with $P_1=4.45$ d and $P_2=1.70$ d. Bottom panel: the original frequency spectrum with $p=0.001$ and 0.005 false-alarm probability thresholds, and cleaned frequency spectrum.

$f_2=0.587\pm0.002\ \mathrm{d}^{-1}$ with $A_1=0.018$, $p_1=0.0009$, and $A_2=0.016$, $p_2=0.006$, respectively. Note that while calculating the values of the false-alarm probabilities and plotting the light curves (Fig. 9), we have pre-whitened each folded light curve from the presence of the other periodicity. The latter frequency is in good agreement with $f=0.58\pm0.01\ \mathrm{d}^{-1}$ found by Moffat et al. (1982). Despite this encouraging result, a search for radial velocity variations provides only weak hints of low-amplitude variability, $K=7$–9 km s^{-1} (comparable to $K=13$ km s^{-1} reported by Moffat et al. 1982), with possible $f_1=0.053$ or $f_2=0.084$, with $\pm0.007\ \mathrm{d}^{-1}$. We do not regard the RV data as a reliable identification of orbital motion in a binary, mainly because the amplitude of the revealed periodicity barely exceeds the averaged accuracy of our measurements, $\sigma(RV)=5.6$ km s^{-1}.

3.8 WR 130 = AS 374

We are not aware of any previous spectroscopy or photometry of this relatively faint star. Our 1994–1995 two-site photometry (Fig. 10) reveals periodicity with $f=0.240\pm0.002\ \mathrm{d}^{-1}$, $A=0.017$, $p=0.020$, which cannot be regarded as significant.

3.9 WR 148 = HD 197406

We have included this WN7 star (WN8h according to Smith et al. 1996) in our survey as a definite SB1 binary system

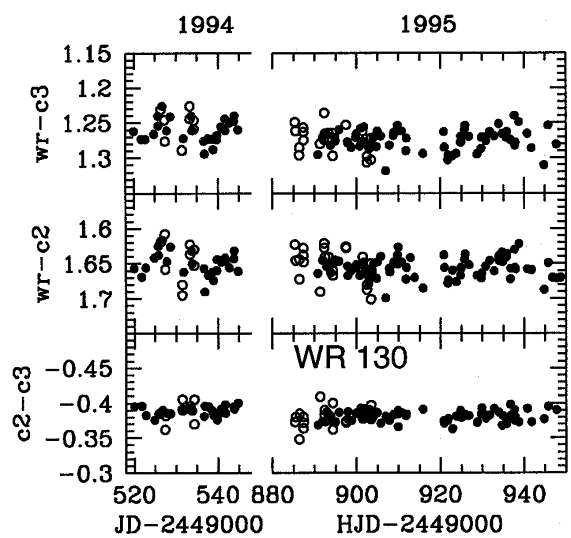

Figure 10. Broad-band (Johnson V) photometry of WR 130 in 1994–1995. Open circles denote the data obtained at Crimea (Ukraine), and filled circles correspond to the San Pedro Martir (Mexico) observations.

with possible compact or early-mid B-type companion (Marchenko et al. 1996) as a kind of reference in our quest for short-period binarity among WN8 stars. We reproduce the 1994–1995 photometry in Fig. 11 along with the

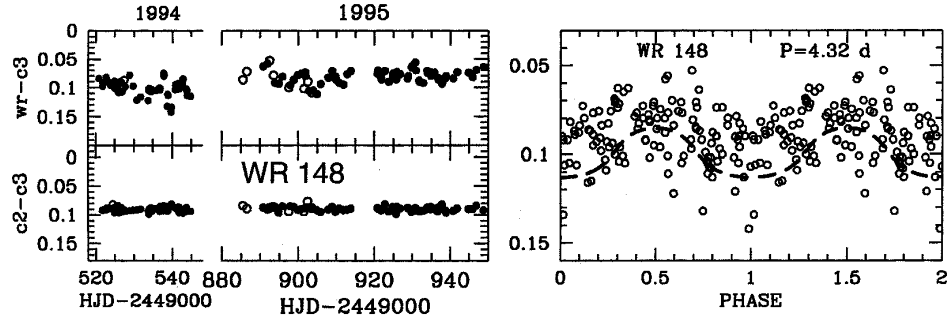

Figure 11. Left-hand panel: broad-band (V) photometry of WR 148 in 1994–1995. Open circles denote the data obtained at Crimea (Ukraine). Filled circles correspond to the San Pedro Martir (Mexico) observations. Right-hand panel: the light curve folded with the well-determined spectroscopic period $P_1 = 4.32$ d; the dashed line denotes the modelled light curve (see text).

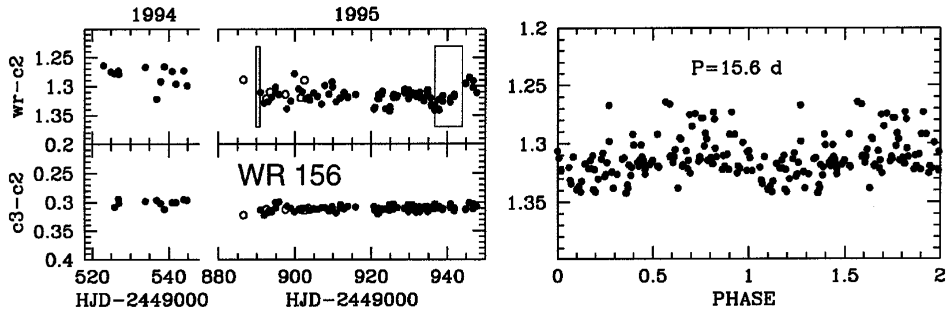

Figure 12. The same as Fig. 5, but for WR 156; $P_1 = 15.6$ d for (wr-c2).

modelled light curve, folded with the binary period $P = 4.3174$ d. Some overall brightening of the star in 1994–1995 as compared to the model light curve deduced from the 1964–1994 observations (cf. Marchenko et al. 1996) can be seen.

3.10 WR 156 = AC + 60°38562

Moffat & Shara (1986) found $f = 0.15\ \mathrm{d}^{-1}$ with higher-frequency aliases, while Lamontagne et al. (1983) detected no orbital motion in this star. Schulte-Ladbeck (1994) describes the polarization spectrum as flat and featureless.

We found the best frequency $f_1 = 0.064 \pm 0.002$, $A = 0.023$, $p = 0.001$ for (wr-c2) and slightly different $f_1 = 0.069 \pm 0.002\ \mathrm{d}^{-1}$, $A = 0.019$, $p = 0.005$ for (wr-c3) in our data set (Fig. 12). Obviously, the modulation may be caused by the specific variability pattern commencing at HJD 244 9924. There are no periodic RV variations (Fig. 8), despite the low detectability level at 6–9 km s^{-1} and high accuracy of the RV derived from the co-aligned spectra via cross-correlation, $\sigma(RV) = 3.3$ km s^{-1}.

4 GENERAL DISCUSSION AND CONCLUSIONS

4.1 Causal relationship(s) between the continuum and spectral variations?

Failing to find any direct relationship between spectral and light variations, we are forced to implement a statistical approach. We simply follow the recipe of Fullerton, Gies & Bolton (1996), calculating the temporal variance spectrum (TVS), with slight modifications. The TVS allows one to estimate the statistical significance of temporal variations across the entire spectrum. At each wavelength (index j) we calculate:

$$TVS_j = \frac{1}{N-1} \sum_{i=1}^{N} \left[\frac{(S/N)_{i\lambda}}{\overline{(S/N)}_{\lambda}} \right]^2 \frac{E_{ij}}{S_{ij}} (S_{ij} - \overline{S}_j)^2 - \sigma_j^2,$$

where N is the number of spectra; $(S/N)_{i\lambda}$ is the S/N ratio of the ith individual, rectified spectrum S_{ij} at a given fixed wavelength λ; $\overline{(S/N)}_{\lambda}$ is the same S/N ratio but for a mean rectified spectrum $\overline{S}_j$; E_{ij} is the continuum fit to the ith raw, non-rectified spectrum; each E_{ij} is normalized, so $E_{i\lambda} \equiv 1.0$. We introduce the value of $\sigma_j = \sqrt{\overline{S}_j}\,\overline{\sigma}$ (Malanushenko 1988) in an attempt to eliminate any spurious details in the TVS introduced by small errors in the wavelength calibration: $\overline{\sigma} = 5$–10 km s^{-1} for the stars in our programme. Under favourable circumstances (for example, when pre-rectifying the target spectra by dividing them by the spectra of simultaneously observed standard stars, and thus minimizing the effects of variable atmospheric extinction), we may substitute $\overline{E}_j/\overline{S}_j$ for E_{ij}/S_{ij}, thus further facilitating the calculations. Additionally, for an assessment of the variability in equivalent width, we use the criterion of Chalabaev & Maillard (1983).

We reproduce in Fig. 13 the mean profiles of 'representative' (i.e., practically blend-free) lines of He II 5412 Å and He I 4471 Å (for WR 123, 124 and 156), He I 5876 for WR 40, as the only available He I line in our spectra) along with overplotted values of $(TVS_j)^{0.5}/\overline{S}_j$, which provide a

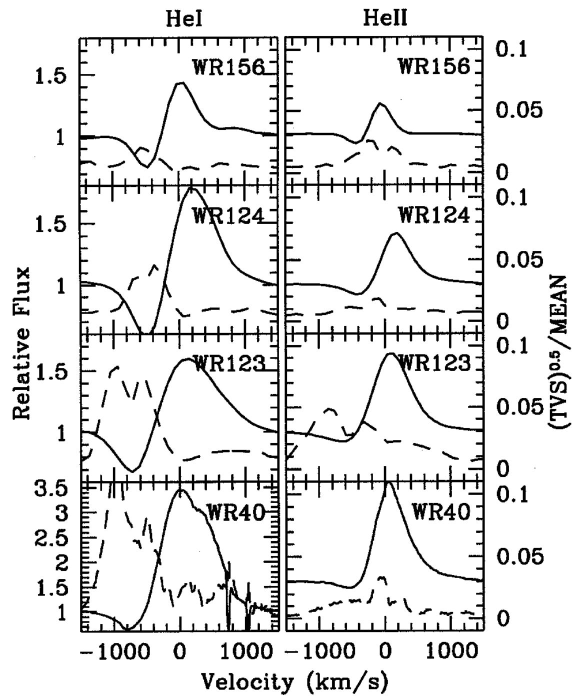

Figure 13. Full lines indicate the mean line profiles of He I 4471 (for WR 123, 124 and 156), He I 5876 (for WR 40, note the different plotting scale for He I line of this star) and He II 5412 (for all four stars), and dashed lines show the value of $(TVS)^{0.5}/MEAN$ (see text).

possibility for intercomparison of TVS_j for the spectral features of different intensities. It is immediately clear that the stars can be ranked in accordance with descending level of line profile variability as follows: WR 123, 40 and 124 and, least active, WR 156. This finding is further supported by the test of EW variations, when considering only non-blended and strong spectral features. In WR 123, the variations of He I 4471, 5876 (both the emission and absorption parts of the P Cygni profile) and absorption part of He II 5412 are significant at the 95 per cent (He II) and ≥99 per cent (He I) level. In WR 40, only He I 5876, but not He II 5412, is variable at the ≥99 per cent level, as well as in WR 124, where only the He I 4471, 5876 lines are significantly variable at 95–99 per cent (slightly lower than in WR 40). WR 156 retains the lowest level, with only the He I 5876 line varying at the ≥99 per cent level. As is clear from Fig. 13, the most vulnerable parts are the P Cygni absorptions of He I, followed by less active absorptions of He II. However, the observed variations are incompatible with the expected behaviour of discrete absorption components (cf. Kaper & Henrichs 1994). There is a tight correlation between the photometric and spectral variations: the higher the level of photometric (i.e., almost pure continuum in the broad-band V filter, with only ~5 per cent of line emission for a typical WNL star) variability, the more 'active' the spectrum. In other words, *the stellar core is triggering (and driving?) the variability, to which the wind is responding.* The same conclusion, although based on less direct evidence, was reached by van Genderen, van der Hucht & Steemers (1987).

Can we somehow clarify the nature of the influence of the core on the wind structure? Our limited data do not provide any clear answer. We only note the perfectly synchronized strengthening of the He I and He II absorptions in WR 40 (Fig. 14) when the continuum flux was on the rise (Fig. 2). On the other hand, in WR 123 the gradual synchronized decrease of the He I, He II absorptions (Fig. 15) occurred during erratic light fluctuations (Fig. 7).

The situation concerning short-term (~hours) spectral variations is even more confusing. Contrary to night-to-night variations with synchronized change of He I and He II absorptions, swift 2–4 h changes of He II are not accompanied by any variations in He I lines (Fig. 16)! This desynchronization can take place if (a) the He I absorption is saturated – which is not the case, at least for WR 123, where the short-term variability occurs when the P Cygni absorption of He I 5876 is far from its maximum strength (compare Fig. 15 to Fig. 16), (b) all observed P Cygni variations occur at $v > v_\infty$, which would imply v_∞ far lower than

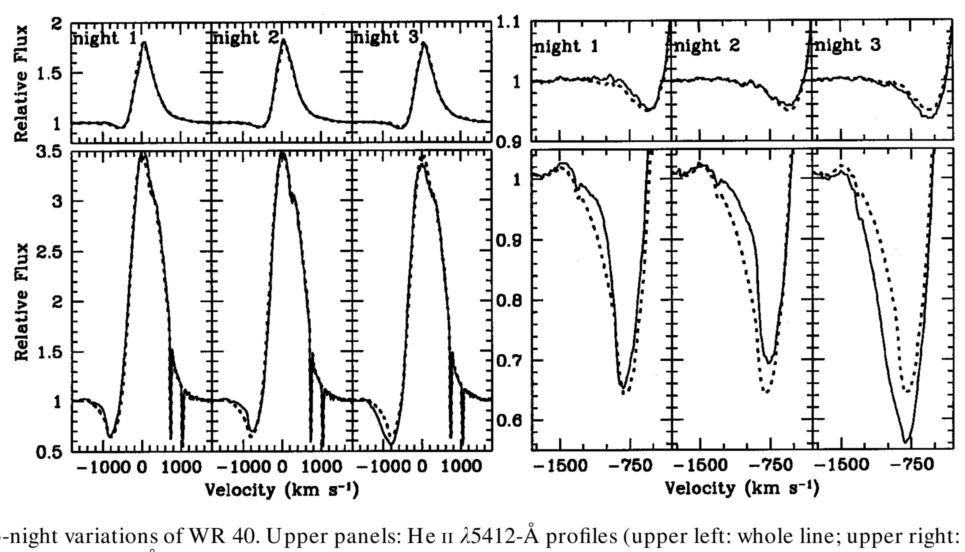

Figure 14. Night-to-night variations of WR 40. Upper panels: He II λ5412-Å profiles (upper left: whole line; upper right: zoomed absorption trough). Lower panels: He I λ5876-Å profiles (lower left: whole line; lower right: zoomed absorption trough). Dotted lines denote the general mean profiles; solid lines indicate the nightly means.

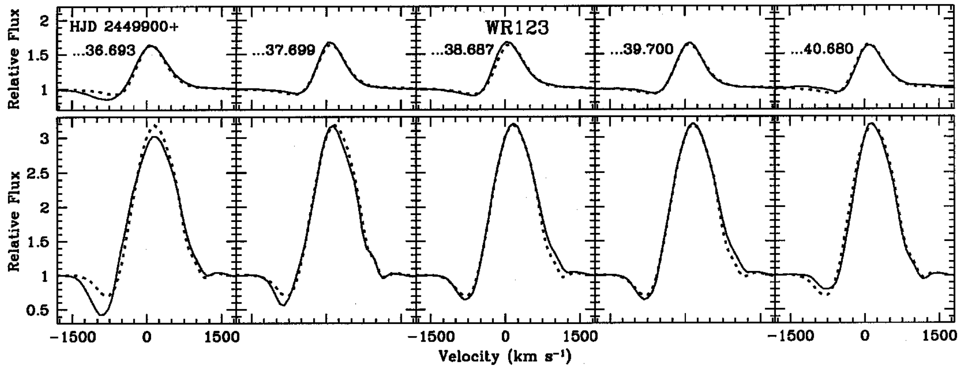

Figure 15. Night-to-night variations of WR 123. Upper panel: He II λ5412-Å profiles. Lower panel: He I λ5876-Å profiles. Dotted lines denote the general mean profiles; solid lines indicate the nightly means.

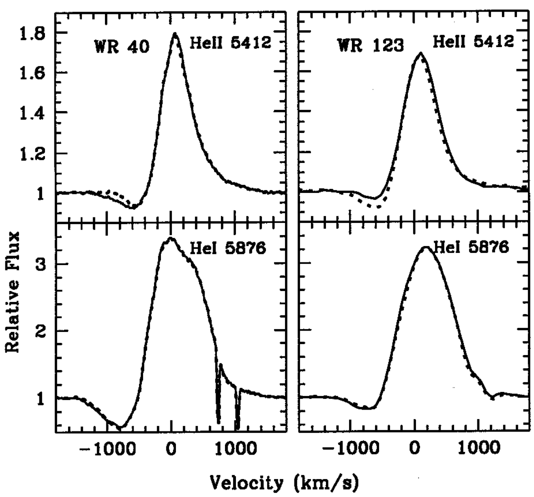

Figure 16. Short-term He II variations. Left-hand panel: He II λ5412 Å versus He I λ5876 Å in WR 40. Right-hand panel: the same, but for WR 123. The profile indicated by a dotted line was obtained 2–4 h after the full-line profile. Note the difference in vertical plotting scales for He I and He II.

usually assigned (Eenens & Williams 1994; Rochowicz & Niedzielski 1995) for these stars, and (c) the last conceivable explanation calls for a non-monotonic velocity law – an assumption which might lead to acceptance of a companion braking the pace of the WR wind acceleration – however, binary behaviour for WR 40 and 123 remains unconfirmed.

4.2 What makes the WN8 stars so violent?

Currently we can consider four conceivable agents that could lead to the high level of variability seen in practically all observed WN8 stars.

(1) Binarity. All periodicities emerging from photometry, spectroscopy or polarimetry are completely inconsistent, with strong epoch dependency and hints of multiperiodicities. As the best and most 'robust' examples of multiperiodic variability confirmed by numerous independent observations, we mention WR 16 (Gosset et al. 1990; Antokhin et al. 1995) and WR 40 (Matthews & Moffat 1994; Antokhin et al. 1995). The only promising cases (besides the very long-period visual binary WR 147) for a binary-like behaviour are WR 40, 66 and 124 (the last being the weakest).

(2) There are numerous and well-documented indications that WR winds are subjected to localized manifestations of 'micro'variability, resulting in rapid growth and outward propagation of density enhancements (wind clumping; cf. Moffat 1996). Can such enhancements account for the observed large photometric and spectroscopic variations? The immediate answer is negative: the observed wind structure is affected *globally* and ~simultaneously, from $\sim v/2_\infty$ to beyond v_∞ (Figs 14–16). If the large variations (up to 0.2 mag) are caused by wind clumping, this should generate polarimetric variations of comparable amplitude. However, the observed polarimetric fluctuations are far smaller: $\sigma(P)_{\rm net}/\sigma(V)_{\rm net} \sim 0.05$–0.1 (Fig. 17; Richardson, Brown & Simmons 1996). This dilemma cannot be resolved by assuming (non-polarized) continuum emission arising from dense blobs: in WR 40 the flux variations show *decreasing* amplitude toward the infrared (Smith, Lloyd & Walker 1985), in contrast to expected growth due to free–free emission; also, the amplitude of the variations *is not* enhanced at the Balmer limit (Matthews & Moffat 1994), despite the presence of some hydrogen in the wind of WR 40.

(3) The most comprehensive search for any relationship between the observed variability of WR stars (expressed statistically as the net rms amplitude for a given star: $\sigma_{\rm net}=[\sigma^2(wr-c_{1(2)})-\sigma^2(c_2-c_1)]^{0.5}$) and any of the fundamental parameters, e.g., M, L, R, $T_{\rm eff}$, $\dot{M}$, v_∞, etc., was performed by Robert et al. (1989) with generally negative results, possibly due to a factor of 2 uncertainty in the basic characteristics. The only clear anticorrelation was found between $\sigma_{\rm net}$ and v_∞, tentatively explained as due to differences in propagation time-scales of 'micro'instabilities (clumps) in the WR wind of a given spectral subgroup: WNL stars as compard to WNE, or WN as compared to WC. We pose the more subtle question: is there any similar dependence between $\sigma_{\rm net}$ and any of fundamental parameters of the WNL stars? Not surprisingly, we fail to find any meaningful correlations between $\sigma_{\rm net}$ and M, L, R, $T_{\rm eff}$ or $\dot{M}$ for WN8 stars. Even far more accurate v_∞ cannot help. However, we do succeed in finding a correlation between all

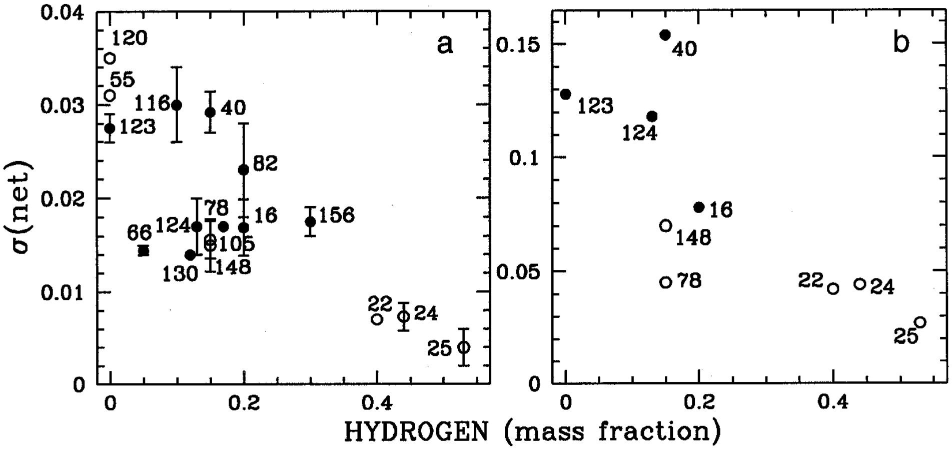

Figure 17. Panel (a): random net photometric variation (in magnitudes) versus hydrogen content, for WN7 (open circles) and WN8 (filled circles) stars. The numbers and spectral subclasses correspond to the designations from the van der Hucht et al. (1988) catalogue. 2σ error bars are provided for multiple $\sigma(net)$ estimations. Panel (b): the same as in panel (a), but for polarimetry [$\sigma(net)$ is in per cent].

available σ_{net} from photometry and polarimetry (Moffat & Shara 1986; Lamontagne & Moffat 1987; van Genderen et al. 1987, 1989; Balona et al. 1989; Robert et al. 1989; Gosset et al. 1990; Antokhin et al. 1995) and the fairly well known relative hydrogen content (Fig. 17) in the stellar wind, as derived by Hamann et al. (1995). The accuracy of the hydrogen content estimation is generally better than 30–50 per cent, when comparing the calculations of Hamann et al. (1995) and Crowther et al. (1995c). The presence of a significant ($H \gtrsim 5$ per cent, by mass) amount of hydrogen may suppress any pulsational instability (Maeder 12985). This may readily explain the general trend seen in Fig. 17. The problem arises when one compares the hydrogen-rich and variable WNL stars to much less variable and practically hydrogen-free WNE/WC stars (Robert et al. 1989): one expects the latter to be violently pulsating in accordance with theoretical predictions. Obviously, the quenching presence of hydrogen must be taken into account while calculating the evolutionary tracks of massive stars, with mass-loss enhanced by vibrational instabilities (Langer et al. 1994).

(4) The most natural source and driver of the variations ($\sim$50 per cent quasi-periodic, $\sim$50 per cent stochastic) might be a stellar core generating multimode oscillations, being further transformed (by either enhancement or 'truncation' of the coherency time? complete evanescence?) and transported by the surrounding optically thick WR wind. However, the type and method of transport must be clarified through detailed calculations, which are far beyond the scope of this paper.

A common feature of all the observed light variations is the relatively high scatter around any folded 'smooth' light curves, sometimes distorting the regular, periodic variations to a limit of undetectability. This scatter may be caused by short-lived, multimode fluctuations. In WR 123, a growth/damping time for the majority of the short-lived oscillations is $\sim$2–3 weeks (Marchenko & Moffat 1997), while some of the frequencies (see Section 3.6) remain stable during the observations.

It is established that in WN7–8 stars the wind performance number ($\dot{M}v_\infty c/L$), as well as the wind density, decreases in stars with higher hydrogen content (Crowther et al. 1995c; Willis 1996). An increased wind density might steepen the ionization gradient, thus increasing the efficiency of radiation pressure as a principal driver of the wind. Can this gain completely account for the relatively high wind performance numbers of the WN7–8 stars with low hydrogen content? The answer awaits detailed modelling. Some additional help might come from the pulsational enhancement of mass-loss, if one incorporates the ionization-induced dynamical instability in accordance with Stothers & Chin (1996).

The characteristic time-scales of the photometrical variations of WNL stars, 1–20 d, are reminiscent of the quasi-periodic variations in massive O stars (de Jager 1980), the direct progenitors of WR stars. However, the peak-to-valley amplitudes of the WNL stars, typically 0.05–0.1 mag, are somewhat larger than those observed among the most massive and luminous O stars, 0.02–0.08 mag. Thus the WNL stars might be placed in between OIII–I stars and LBVs (referring to their microvariations) in the maximum light amplitude diagram of van Genderen (1989). Combining very high activity with relatively high luminosity and detectable amount of hydrogen in the stellar envelope, as well as accounting for the suggested direct link between LBV and WNL evolutionary phases (Langer et al. 1994; Crowther et al. 1995c), one is inclined to label WN8 stars the 'quiescent LBVs' of the WR population.

ACKNOWLEDGMENTS

We appreciate excellent support and good will of the San Pedro Martir Observatory staff during our long observing run. AFJM thanks NSERC (Canada) and FCAR (Quebec) for financial assistance. TE is grateful to the Evangelisches Studienwerk (supported by the German Government) for continuing financial aid. We thank I. Antokhin and C. Robert for providing us with the reduced photometry of

WR 123, 124, 130, 148 and 156 (I. Antokhin) and rectified spectra of WR 40 (C. Robert). We gratefully acknowledge usage of the STScI DSS for precise measurements of stellar coordinates.

REFERENCES

Abbott D. C., Bieging J. H., Churchwell E., Torres A. V., 1986, ApJ, 303, 239
Antokhin I. I., 1987, Astron. Tsirk., 1489, 5
Antokhin I. I., Cherepashchuk A. M., 1989, Pis'ma Astron. Zh., 15, 701
Antokhin I. I., Bertrand J. F., Lamontagne R., Moffat A. F. J., Matthews J. M., 1995, AJ, 109, 817
Balona L. A., Egan J., Marang F., 1989, MNRAS, 240, 103
Breger M., 1989, Commun. in Asteroseismology, No. 6, Austrian Acad. Sci.
Chalabaev A., Maillard J. P., 1983, A&A, 127, 279
Conti P. S., Massey P., 1989, ApJ, 337, 251
Crawford I. A., Barlow M. J., 1991, A&A, 249, 518
Crowther P. A., Smith L. J., 1997, A&A, in press
Crowther P. A., Hillier D. J., Smith L. J., 1995a, A&A, 293, 172
Crowther P. A., Hillier D. J., Smith L. J., 1995b, A&A, 293, 403
Crowther P. A., Smith L. J., Hillier D. J., Schmutz W., 1995c, A&A, 293, 427
de Jager C., 1980, The Brightest Stars. Reidel, Dordrecht
Eenens P. R. J., Williams P. M., 1994, MNRAS, 269, 1082
Fullerton A. W., Gies D. R., Bolton C. T., 1996, ApJS, 103, 475
Gosset E., Vreux J.-M., Manfroid J., Remy M., Sterken C., 1990, A&AS, 84, 377
Hamann W.-R., Koesterke L., Wessolowski U., 1995, A&A, 299, 151
Kaper L., Henrichs H. F., 1994, in Moffat A. F. J., Owocki S. P., Fullterton A. W., St-Louis N., eds, Instability and Variability of Hot Stellar Winds, Kluwer, Dordrecht, p. 115
Lamontagne R., Moffat A. F. J., 1987, AJ, 94, 1008
Lamontagne R., Moffat A. F. J., Seggewiss R., 1983, ApJ, 269, 596
Langer N., Hamann W.-R., Lennon M., Najarro F., Pauldrach A. W. A., Puls J., 1994, A&A, 290, 819
Leitherer C., Chapman J. M., Koribalski B., 1995, ApJ, 450, 289
Leitherer C., Chapman J. M., Koribalski B., 1997, ApJ, 481, 898
Maeder A., 1985, A&A, 147, 300
Maeder A., 1996, in Vreux J.-M. et al., eds, Wolf–Rayet Stars in the Framework of Stellar Evolution. Université de Liège, p. 39
Malanushenko V. P., 1988, Trudu Tartusskoii Astrofiz. Observatorii, 92, 60
Marchenko S. V., Moffat A. F. J., 1997, ApJ, submitted
Marchenko S. V., Antokhin I. I., Bertrand J. F., Lamontagne R., Moffat A. F. J., Matthews J. M., Piceno A., 1994, AJ, 108, 678
Marchenko S. V., Moffat A. F. J., Lamontagne R., Tovmassian G. H., 1996, ApJ, 461, 386
Massey P., Conti P. S., 1980, ApJ, 242, 638
Matthews J. M., Moffat A. F. J., 1994, A&A, 283, 493
Moffat A. F. J., 1989, ApJ, 347, 373
Moffat A. F. J., 1996, in Vreux J.-M. et al., eds, Wolf–Rayet Stars in the Framework of Stellar Evolution. Université de Liège, p. 199
Moffat A. F. J., Isserstedt J., 1980, A&A, 85, 201
Moffat A. F. J., Shara M. M., 1986, AJ, 92, 952
Moffat A. F. J., Lamontagne R., Seggewiss W., 1982, A&A, 114, 135
Moffat A. F. J. et al., 1997, A&A, in press
Morris P. W., Eenens P. R. J., Hanson M. M., Conti P. S., Blum R. D., 1996, ApJ, 470, 597
Niemela V. S., 1991, in van der Hucht K. A., Hidayat B., eds, Proc. IAU Symp. 143, Wolf–Rayet Stars and Interrelations with Other Massive Stars in Galaxies. Kluwer, Dordrecht, p. 201
Niemela, V. S., Shara M. M., Wallace D. J., Zurek D. R., Moffat A. F. J., 1997, AJ, in press
Nota A., 1995, in van der Hucht K. A., Williams P. M., eds, Proc. IAU Symp. 163, Wolf–Rayet Stars: Binaries, Colliding Winds, Evolution. Kluwer, Dordrecht, p. 78
Rauw G., Gosset E., Manfroid J., Vreux J.-M., Claeskens J.-F., 1996, A&A, 306, 783
Richardson L. L., Brown J. C., Simmons J. F. L., 1996, A&A, 306, 519
Robert C., 1992, Thèse de Doctorat, Université de Montréal
Robert C., Moffat A. F. J., Bastien P., Drissen L., St-Louis N., 1989, ApJ, 347, 1034
Roberts D. H., Lehar J., Dreher J. W., 1987, AJ, 93, 968
Rochowicz K., Niedzielski A., 1995, Acta Astron., 45, 307
Scargle J. D., 1982, ApJ, 263, 835
Schulte-Ladbeck R. E., 1994, in Moffat A. F. J., Owocki S. P., Fullterton A. W., St-Louis N., eds, Instability and Variability of Hot Stellar Winds. Kluwer, Dordrecht, p. 347
Smith L. F., Shara M. M., Moffat A. F. J., 1996, MNRAS, 281, 163
Smith L. J., Lloyd C., Walker E. N., 1985, A&A, 146, 307
St-Louis N., Moffat A. F. J., Drissen L., Bastien P., Robert C., 1988, ApJ, 330, 286
Stothers R. B., Chin C., 1996, ApJ, 468, 842
Tamblyn P., Rieke G. H., Hanson M. N., Close L. M., McCarthy D. W. Jr, Rieke M. J., 1996, ApJ, 456, 206
van der Hucht K. A., 1992, A&AR, 4, 123
van der Hucht K. A., Hidayat B., Admiranto A. G., Supelli K. R., Doom C., 1988, A&A, 199, 217
van Genderen A. M., 1989, A&A, 208, 135
van Genderen A. M., van der Hucht K. A., Steemers W. J. G., 1987, A&A, 185, 131
van Genderen A. M., van der Hucht K. A., Bakker P. R., 1989, A&A, 224, 125
van Genderen A. M. et al., 1991, in van der Hucht K. A., Hidayat B., eds, Proc. IAU Symp. 143, Wolf–Rayet Stars and Interrelations with Other Massive Stars in Galaxies. Kluwer, Dordrecht, p. 129
Vreux J.-M., Andrillat Y., Biémont E., 1990, A&A, 238, 207
Williams P. M., van der Hucht K. A., Thé P. S., 1987, A&A, 182, 91
Williams P. M., Dougherty S. M., Davis R. J., van der Hucht K. A., Bode M., Setia Gunawan D. Y. A., 1997, MNRAS, in press
Willis A. J., 1996, Ap&SS, 237, 145